| 1.Report No.<br>TxDOT 7-3969-1 | 2. Government Accession No. | 3. Recipient's Catalog No. | |
|---|---|---|---|
| 4. Title and Subtitle<br>Investigation of Short Range Sensing Devices for Use in Non-Destructive Pavement Evaluation | | 5. Report Date<br>October 2000<br>6. Performing Organization Code | |
| 7. Author(s)<br>Richard Liu, Xuemin Chen, Xinhua Gan, Jing Li, Yong Rao, Huichun Xing and Renyue Liang | | 8. Performing Organization Report No.<br>3969-1 | |
| 9. Performing Organization Name and Address<br>Department of Electrical and Computer Engineering<br>University of Houston<br>4800 Calhoun Rd.<br>Houston, TX 77204-4793 | | 10. Work Unit No.<br>11. Contract or Grant No.<br>7-3969 | |
| 12. Sponsoring Agency Name and Address<br>Research and Technology Implementation Office<br>Texas Department of Transportation<br>P. O. Box 5080<br>Austin, Tx 78763-5080 | | 13. Type of Report and Period Covered<br>Final Report<br>14. Sponsoring Agency Code | |
| 15. Supplementary Notes<br>Project conducted in cooperation with the Texas Department of Transportation and the Federal Highway Administration | | | |
| 16. Abstract:<br>In this project we investigate many different short-range sensors used in pavement micro and macro texture measurement. Two categories of sensors are researched: light wave-based sensors and electromagnetic (EM) wave based sensors. Light wave based sensors include laser triangulation with feed back control. EM sensors include microwave and millimeter wave macro texture detectors. The laser sensor is prototyped and lab-tested. Limited field tests have been performed. This prototype laser sensor includes laser transceivers, data acquisition system, and associated software. Tested results show that the laser sensor is able to measure both macro and micro textures of the pavements. This report briefly discusses basic operation principles of the laser system, implementation details and software development. The EM sensors are based on microwave scattering from a rough surface. Macro texture information can be extracted form mathematics computation using data measured by the EM sensor. Several frequency bands were investigated including 10 GHz band, 35 GHz band, and 90 GHz band. The tested results show that microwave and millimeter waves are very sensitive to pavement textures. Prototype EM sensor were constructed and lab tested. Theoretical discussions of the EM sensor are given in this report. Several tested cases are also presented. | | | |
| 17. Key Words<br>Laser, micro texture, macro texture, laser triangulation, position sensitive device, microwave remote sensing, millimeter waves, inversion | 18. Distribution Statement<br>No restrictions. | | |
| 19. Security Classif. (of this report)<br>Unclassified | 20. Security Classif. (of this page)<br>Unclassified | 21. No. of Pages<br>90 | 22. Price |

Form DOT F 1700.7 (8-72) Reproduction of completed page authorized

This form was electrically by Elite Federal Forms Inc.

**Final Report**

# Investigation of Short Range Sensing Devices for Use in Non-Destructive Pavement Evaluation

Richard Liu
Associate Professor, Principle Investigator

Xuemin Chen
Xinhua Gan
Jing Li
Research Associates

Yong Rao
Huichun Xing
Renyue Liang
Jiangtao Lin
Research Assistants

Project No.: TxDOT P7-3969
Conducted in Cooperation With The
Texas Department of Transportation
and the
Federal Highway Administration
TxDOT Project Director: Brian Michalk
TxDOT Project Coordinator: Carl Bertrand

# DISCLAIMERS

The contents of this report reflect the views of the authors who are responsible for the facts and accuracy of the data presented herein. The contents do not necessarily reflect the official views or policies of the Texas Department of Transportation. This report does not constitute a standard, specification or regulation.

University of Houston
4800 Calhoun Rd.
Houston, TX 77204

# Table of Contents

# List of Figures

# List of Tables

# CHAPTER 1: INTRODUCTION

## 1.1 PROJECT OVERVIEW

Highway skid number is largely dependent on the texture of the pavement. For many years, TxDOT uses skid truck to measure skid number directly. The skid truck is a trailer with a standard weight. During the skid measurement, brake is applied to the trailer. This measurement is direct and accurate. However, measurement speed is limited and frequent traffic slow down is inevitable. For years, TxDOT has been pursuing alternative skid measurement methods using laser and other NDT tools such as laser and microwave. Two major components are included in order to achieve a non-contact skid measurement. The first component is to investigate short-range sensors that are sensitive to micro and macro texture. The second one is to relate the skid number to the measured data. In this project, the emphasis is on the sensor development. TxDOT intend to use the non-contact skid measurement device for network level pavement data collection. Commercial laser is expensive and measurement speed is limited to 40 – 55 miles per hour. High speed and low-cost laser system is desired for network level skid measurement. In this project, we investigate several texture sensing devices including a high speed and low cost laser sensor for micro and macro texture detection, and a microwave sensor for macro texture measurement.

The outcome of this research includes several prototype pavement texture measurement devices: a laser texture sensor which runs at 178 kHz allowing highway speed measurement, and a microwave macro texture sensor that is sensitive to macro texture. We also investigated the relations between texture data with skid number. Preliminary results show that the skid number is a non-linear function of the texture parameters.

# CHAPTER 2 LITERIATURE REVIEW

## 2.1 BACKGROUD

The highway pavement texture is an important parameter in the condition assessment of the pavement [1]. The texture measurement includes the microtexture and macrotexture measurements. The macrotexture can be obtained from processing data measured for microtexture. The average highway texture is about 0.5 mm in size, and the accuracy required for microtexture measurement is in 0.1-mm range. ASTM MPD and ETD specify microtexture < 0.5 mmwavelength. Does not specify amplitude, or vertical displacements.

Currently, TxDOT uses laser sensor and high frequency ultrasound sensors for the rut bar and profile measurements. Texture measurement using laser sensor is limited to 40-50 miles per hour. Assuming we meet nyquist for 0.25 mm sample spacing, we can go 50 mph. However, our data correlates at highway speeds.

Due to the rapid development of EM sensors by ex-defense industries, the EM Sensors have great potential to meet the current TxDOT needs. Two types of EM sensors were investigated in this project: the millimeter-wave radar and centimeter radar. The millimeter-band electromagnetic waves behave very similarly to the lasers in terms of resolutions, but unlike lasers, the EM sensors are not very sensitive to the standoff distances. The EM sensors have been widely used in satellite and airborne remote sensing at a standoff distance of several hundreds miles or more with a resolution of several inches [2,3,4]. Another obvious advantage of the EM sensors is the ability of depth investigation. The EM waves can propagate into the road surface for a short distance, which implies that there is a possibility to find other parameters of the road surface by processing the data from EM sensors.

There are three light sensors that can be used for texture measurement: the CCD sensors, the coherent and non-coherent laser sensors, and the inferred distance sensors. The laser displacement measurement is based on the interference between the transmitted and reflected or scattered light by the road surface [5]. Because of the extremely short wavelength of the laser, the accuracy can be very high. On the other hand, the receiver becomes very complicated and expensive [5, 6]. Similar accuracy can be obtained by using charge-coupled devices (CCDs) with a laser transmitter. Laser transmitters have a very narrow beam width and are inexpensive. CCDs are used as receivers for the laser spot. Two CCD elements can be used to locate the laser spot with an accuracy of several tenth of a millimeter [7]. CCDs and the laser source are low price devices with a high accuracy. The combination of a CCD with a central laser source will solve the problems of high cost and close-sensing ranges, which are widely used in robot and computer vision systems [8]. Alternate to CCD sensors, position sensitive device (PSD) can be used to detect light scattering from rough surface. For more accurate measurement, coherent laser system can be used. Comparing to coherent laser system, none-coherent laser system are less accurate. The reason is that the coherence laser system uses a reference laser and the system measure the phase difference with the reference laser. Since the wavelength of the laser light is very short, so the coherence laser system is more accurate. On the other hand, non-coherent laser systems are more reliable and less expensive. To obtain a higher accuracy using the non-coherent lasers, data processing is necessary [9, 10]. After carefully study all the options, the researcher decided to use non-coherent, PSD based laser measurement system for texture sensor to reduce cost. Challenges will be accuracy and measurement speed.

# CHAPTER 3 DEVELOPMENT OF LASER TEXTURE MEASUREMENT SYSTEM

## 3.1 THEORY OF LASER TRIANGULATION METHOD

The macro/micro measurement system consists of three subsystems: Optical system, electronic circuits and data acquisition, and processing unit, as shown in Figure 3.1.

Figure 3.1 Macro/Micro measurement system.

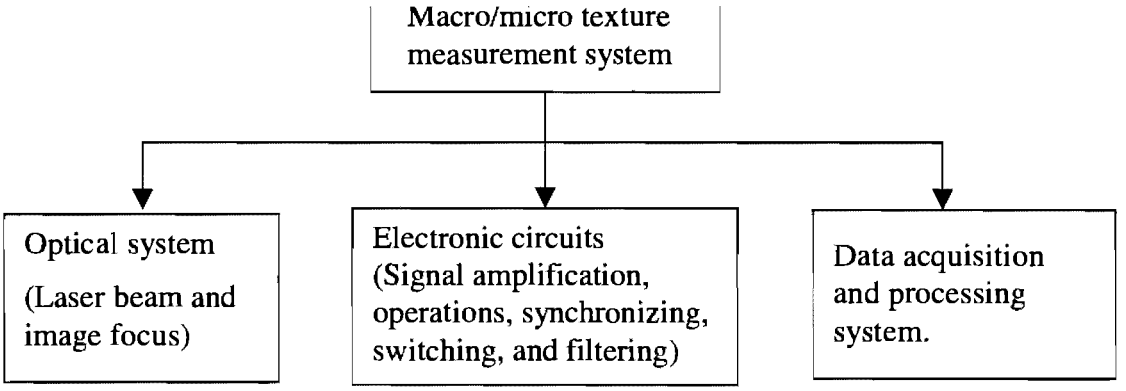


The following describes the design of the optical system. Detailed descriptions of the hardware implementation can be found in Chapter 4.

## 3.2 OPTICAL SYSTEM DESIGN

The discussion of ranging sensing techniques presented in Chapter 2 indicates that to acquire texture (position) information of measuring objects, the laser-based triangulation method is the one that provides the most simplicity, flexibility and the greatest speed of operation. In this chapter, the discussion focuses on the implementation theory of the triangulation method.

### 3.2.1 INTRODUCTION

The triangulation method is a most widely used approach in modern industry, especially in surface inspection [11,12,13]. Having the advantages of low-cost, simplicity, robustness and good resolution, the laser-optic triangulation has been widely applied to both profiling and gauging applications [12-33]. It provides the capabilities of high speed, non-contact, and high accuracy.

There are several parameters pertaining to a range sensor that indicate the system performance. These parameters include sampling rate, dynamic range of depth measurement and measurement resolution (accuracy).

The laser-based triangulation system consists of a laser diode, an optical positioning system, a signal generation circuitry and a data acquisition and analysis system.

### 3.2.2 TRIANGULATION PRINCIPLE

Two components constitute the optical system of the triangulation range sensing method: the laser beam generating mechanism and the position sensitive detector (PSD) system. In the following section the mathematical formation of triangulation method is presented.

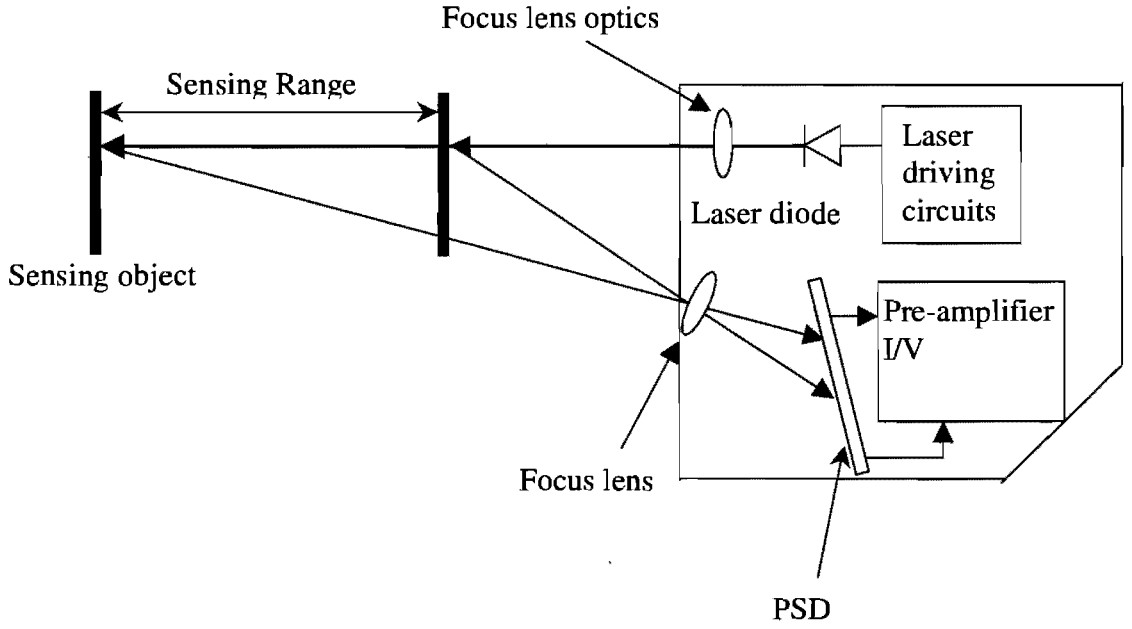


Figure 3.2. Laser-based triangulation system.

The concept of optical triangulation is illustrated in Figure 3.1. In this technique, a collimated laser beam illuminates the measurement surface. The target surface reflects the beam, which is then focused on the PSD, and forms a beam spot. The beam spot moves on the PSD as the surface height changes. The displacement of the surface can then be determined by detecting the movement of the beam spot.

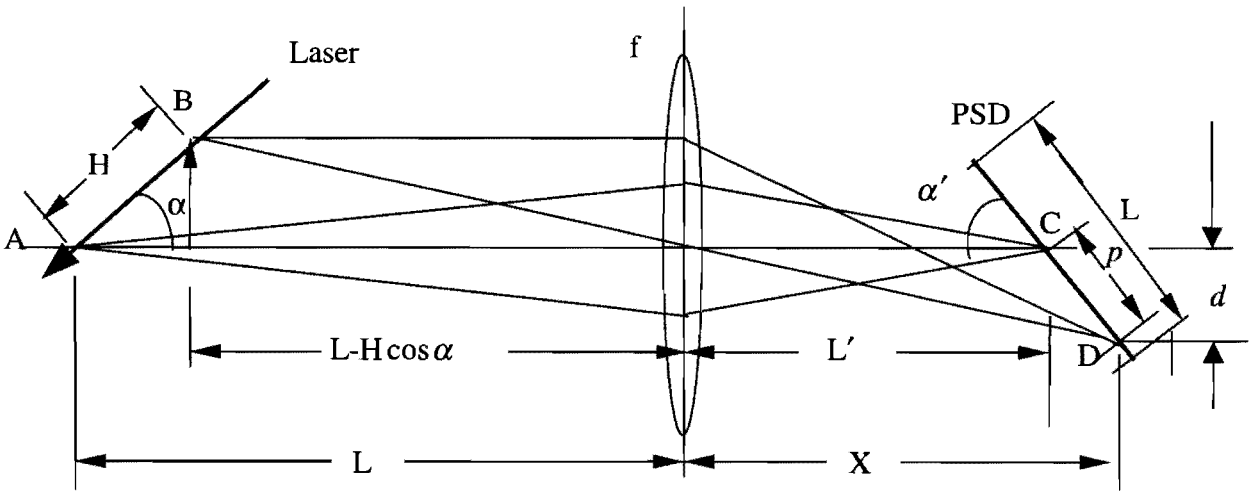


Figure 3.3 Triangulation principle.

Figure 3.2 illustrates the geometry of image formation. Assume that the laser beam intercepts the optical axis at point A and the virtual image of A is located at point C (on the axis). Image B corresponds to point D. According to the law of image focusing, the following relationships can be established:

$$\frac{1}{f} = \frac{1}{L} + \frac{1}{L'} \tag{3.1}$$

and

$$\frac{1}{f} = \frac{1}{L - H\cos\alpha} + \frac{1}{X}, \tag{3.2}$$

where H is the change of height (from point A to point B) and $\alpha$ is the formation angle (viewing angle) of the image. From Equations (3.1) and (3.2), L′ and X can be expressed as Equation (3.3) and Equation (3.4)

$$L' = \frac{Lf}{L - f} \tag{3.3}$$

and

$$X = \frac{f(L - H\cos\alpha)}{L - H\cos\alpha - f}. \tag{3.4}$$

The heights of point B and its image D comply with the law of image magnification, which states as Equation (3.5)

$$\frac{d}{H\sin\alpha} = \frac{X}{L - H\cos\alpha}. \tag{3.5}$$

where $d$ is the height of image. Substitute X using Equation (3.4), then $d$ can be expressed as:

$$d = \frac{fH\sin\alpha}{L - H\cos\alpha - f}. \tag{3.6}$$

To find out $\alpha'$, the angle of PSD with the main optical axis, have

$$X - L' = \frac{f(L - H\cos\alpha)}{L - H\cos\alpha - f} - \frac{fL}{L - f}$$

$$= \frac{f^2 H\cos\alpha}{(L - f)(L - H\cos\alpha - f)}. \tag{3.7}$$

The slope of line segment CD therefore is

$$\tan\alpha' = \frac{d}{X - L'} = \frac{fH\sin\alpha}{L - H\cos\alpha - f} \times \frac{(L - f)(L - H\cos\alpha - f)}{f^2 H\cos\alpha'}$$

$$= \frac{(L - f)}{f}\tan\alpha$$

$$= const. \tag{3.8}$$

The position data $p$ can be read out directly from the circuitry output. From Equation (3.9)

$$\frac{1}{f} = \frac{1}{H\sin\alpha} + \frac{1}{p\sin\alpha'}, \tag{3.9}$$

$H$ can be calculated by Equation (3.10)

$$H = \frac{fp\sin\alpha'}{(p\sin\alpha' - f)\sin\alpha} \tag{3.10a}$$

or

$$p = \frac{Hf\sin\alpha}{(H\sin\alpha - f)\sin\alpha'} \tag{3.10b}$$

In the macro/micro system design, two factors need to be taken into account: the choice of the imaging lens and the distance between from the imaging lens and the object. The intensity of the reflected light is very weak (in μW). To increase the energy from the reflected light, a lens with a bigger size is adopted. Therefore, the spot focused on PSD is strong enough and the PSD generates stable signals at low noise level. However, the mounting requirement limits the size of the lens. It is impossible to get a large lens in short focus without imaging distortion. The distance from the lens to the object is a major parameter affecting the light energy collected by imaging lens. The smaller the distance, the more energy from the spot enters the imaging lens. In design, a diameter of 50mm plano-convex lens (focus 50mm) is utilized as the imaging lens. The distance from the lens to the pavement is set to 50mm (stand off distance). Therefore, the parameters in the formulas from Equation (3.1) through Equation (3.10) are $\alpha$ = 35°, $L$= 11mm, $\alpha'$ = 40.038° and $L'$ = 91.034mm respectively.

## 3.3 LASER BEAM

### 3.3.1 INTRODUCTION

Laser has had a tremendous impact on various fields in science and technology. It is now being widely used as a precise light source in medicine, communications, national defense, and measurement industries. Many types of lasers are commercially available with a large range of output wavelengths and power, such as HeNe, ruby, Nd-YAG, Nd-Glass, CO2, dye, and the semiconductor diode.

Most laser systems are expensive and have complicated structures. The appearance of laser diode can change this situation. Based on the features of the macro/micro measurement system, the low cost, small size, low power and simple to use semiconductor laser (laser diode) is adopted in the system.

### 3.3.2 FEATURES OF LASER

Lasers take many different forms and have many differing characteristics, such as the wavelength, output power, duration of emission (pulsed or continuous), beam divergence, size and coherence.

Wavelength is a fundamental characteristic of the light. Each type of laser emits a characteristic wavelength. In triangulation application, the visibility and detector sensing range should be taken into account. A near infrared laser, with a wavelength of 780nm, is employed in the system. There are many reasons for choosing this laser. First of all, this characteristic wavelength is the closest to the sensitive peak of the PSD, which is 900nm. Secondly, the brightness of this infrared laser is not strong due to its characteristic wavelength near the scope of infrared band, which reduces the impairment to eyes. Thirdly, its visibility lets this semiconductor laser beam spot and the system is easy to be setup and aligned.

The output power is a major factor that affects the accuracy of the measurement system. In the triangulation method, the measurement is mainly implemented by the collection of reflected light intensity, which plays a critical role in the system. In Chapter 4, one of the system designed features regarding how to keep the output power constant is addressed. This issue is to solve the problem of the measurement on different color and shape surfaces.

In the system, a continuous output laser is required. It is driven in the pulsed mode to meet the requirement of the special design of the measurement system for this study.

### 3.3.3 LASER BEAM

The beam projected onto the surface must have a uniform intensity profile over the range of elevations to be measured. A single-mode laser beam and high-quality projection optics are required.

Like other laser diodes, it has the problem of divergence. A parallel beam is desired in the profiling measurement. To get an absolutely parallel beam, a complicated optical system needs to be built up. The shape of the laser source, the output power loss, the measurement accuracy and the simplicity should be considered sophisticatedly. Some trade-off should be reached. In our system design, a laser diode of 70mW, divergence of 0.49 and 5.6mm package (smaller light source) is chosen. It also has a good heat dissipation capability.

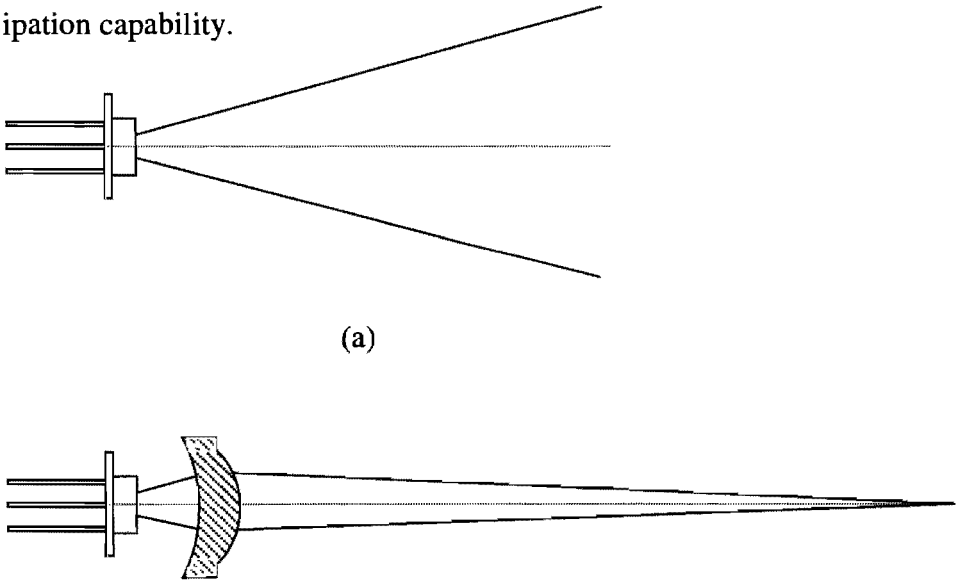

(a)

(b)

Figure 3.4 (a) Laser diode and beam divergence.

(b) Beam collimation with an aspheric lens and focus.

Figure 3.4 (a) illustrates the laser diode and the generation of the beam. The source of the laser diode is usually elliptical. A spherical lens cannot focus the divergent beam into an exact circular beam. Whereas, the aspherical lens can collimate the non-circular light source into an approximately circular beam if the light source is small and the focused distance is moderate. However, if a very high accuracy is required, an absolutely circular laser beam is definitely needed. A lens group should be combined to collimate the beam. For example, for a 250mW laser diode (9mm package), its source is a 2.0×0.3mm line shape, which needs an aspherical lens to focus the divergent lights into a line shape, and then another cylindrical lens is needed to focus the linear image into a circular spot (approximately). The level of complication of the lens grouping depends on the requirement of accuracy.

For this study, an aspherical lens is employed to generate the circular spot as shown in Figure 3.4 (b). Because the focus length is about 25cm and the measurement range is set to 20mm, an approximate circular beam can be obtained within that scope. The spot size is adjusted to about 0.4~0.7mm in diameter. It should be aware that the diameter of the spot size should not be allowed to be arbitrarily too small. If the spot size is adjusted to a very small size, the surface texture will cause the detection system to be oversensitive to the micro texture. On the other hand, the larger spot size will not react to bigger particles due to blockage. However, if the spot size is too large, the fine texture will be ignored by the system. The surface range (position) with variable reflectivity within the laser spot size can result in intensity distributions (shift of the centroid). In this way, the finer displacement can be detected.

## 3.4 POSITION SENSING DETECTOR

Basically, there are two kinds of detectors suitable for the high speed and high accuracy position sensing detection: one is couple charged device (CCD) and the other is position sensitive detector (PSD).

### 3.4.1. CCD

CCD, used in triangulation measurement, can detect the peak value of the light quantity distribution of the beam spot focused on a CCD sensing array (linear) and then determine the precise target position.

CCD has its advantages and disadvantages. The advantages include the directly digitized output data, comparatively independent of light spot focus, and its easy process. The disadvantages include the low scanning rate and the limited resolution. For example, the linear scan CCD with the scanning rate 33MHz (256 pixels) has a reading rate of 128.9kHz. For the 33MHz scanning rate (512 pixels), its reading rate is 64.5kHz. For 40MHz (4096 pixels), its reading rate 9.76kHz. Only the 33MHz/256 pixels linear scan CCD meets our sampling rate requirement, i.e. 107kHz.

The CCD's pixel dimension is 14μm×14μm, which determines the smallest measurement resolution. It limits the extensibility of the measurement system. Furthermore, the total sensitive length of the 256-pixel line scan CCD is 256×14μm = 3.6mm, or a little bit longer, if considering the gaps between pixels. This sensitive length is another limitation on the measurement range.

### 3.4.2 PSD

The silicon opto-electronic sensor PSD can provide continuous position data of light spots traveling over their photosensitive surfaces. Compared to the discrete-element detectors, PSD has many advantages such as high position resolution (7μm), high-speed response time (0.7μs, i.e. 148kHz (5v) ~ 400kHz (15v)), simultaneous measurements of position and intensity.

The PSD consists of monolithic, PIN (P, I and N layers) photodiodes with a uniform resistive surface. Figure 3.5 illustrates the principle of PSD.

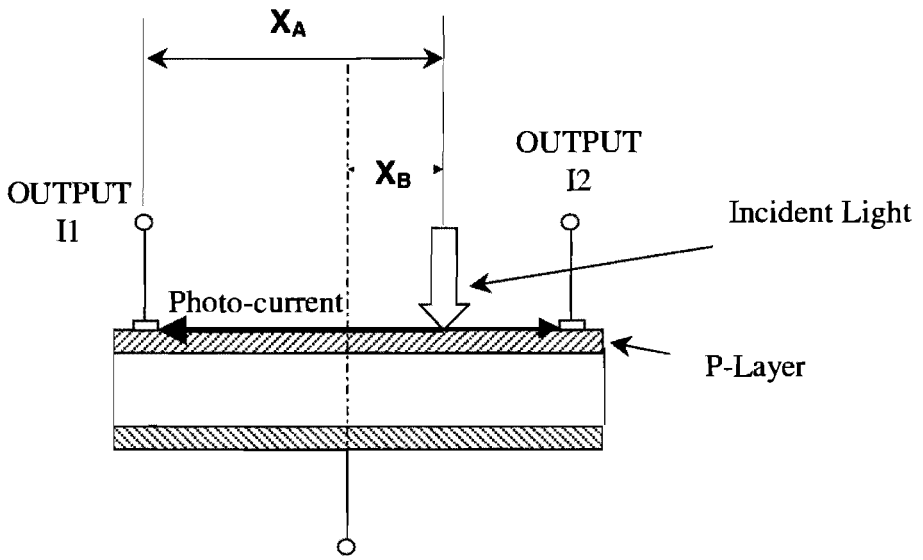


Figure 3.5 PSD (position sensitive detector) principle diagram.

When a light spot falls on the PSD, an electric charge proportional to the light energy is generated at the incident position. This electric charge is driven through the resistive P-layer and collected by the electrodes. Since the resistivity of the P-layer is uniform, the photocurrent collected by an electrode is inversely proportional to the distance between the incident position and the electrode. It is possible to obtain the following formulas for the photo-currents *I1* and *I2* collected by the electrodes, where *L* and *I0* respectively stand for the electrode inter-distance and the total photo-current,

$$\frac{I_2 - I_1}{I_1 + I_2} = \frac{2x_A}{L} \tag{3.11}$$

or

$$x_A = \frac{L}{2} \times \frac{I_2 - I_1}{I_1 + I_2}. \qquad (3.12)$$

From the difference or the ratio of *I1* and *I2,* the incident position of light can be found by the above formulas in respect to the energy of incident light [14]. The system circuit design is based on the above principle.

# CHAPTER 4 MEASUREMENT SYSTEM HARDWARE AND TECHNOLOGY

This chapter describes the hardware design of the position sensing system for producing the position (texture) data.

## 4.1 GENERAL DESIGN FEATURES

The hardware circuitry incorporates analog and digital circuits for the signal discrimination and processing, and operates under pulsed mode with linear PSD (position sensitive detector). Pulsed operation enables a reliable position measurement of the light spot, even in the presence of background light.

The system pulse frequency is set to 175kHz, which exceeds the original design objective –107kHz. This higher frequency guarantees the system has quick speed time to handle the signal variation caused by the background fluctuations.

The use of opto-electronic components involves the signal coupling and the weak signal pre-amplification. Arithmetic operations, such as subtraction, addition and division, are employed to process the signals. The use of sample/hold and subtraction operation aims to extract the signal from the background.

Like most other analog circuits, filtering technologies are applied to restraint the noise generated in circuits. The sequential logic is utilized to straighten out the signal, which is critical to the stable input signal of the proportional, integral and derivative (PID) control loop. The PID control takes the scattered signal form the PSD output and process the signal. Based on the signal characteristics, PID controls the laser intensity. PID control loop guarantees a precise control and a quick response in the measurements

regardless of the changes in target color, surface characteristics and other fluctuation in reflected light intensity.

The laser diode is driven by a power amplifier. The protection circuit is intended for avoiding any damages to the laser diode under abnormal operations or malfunctions.

## 4.2 SYSTEM HARDWARE AND TECHNOLOGY

### 4.2.1 CIRCUITRY FRAME

Figures 4.1 and Figure 4.2 present the block diagrams that describe all functional parts in the measurement circuitry design.

### 4.2.2 SIGNAL MATCHING/COUPLING AND AMPLIFICATION

A PSD is a two-layer photoelectric component. When light impinges its surface, the photo-current *I1* and *I2* will generate and flow out through its two electrodes. Due to the application of laser pulse-driven method, currents are periodically alternated at the output electrodes at the frequency of 175kHz. Capacitors are the best couplers employed to convey the signals to the pre-amplifier. However, the value of the capacitor impacts the balance of the circuit, especially when system works in a large range stand off distance. Properly chosen, the capacitor can enhance the performance of the system. Another advantage of using capacitors is to isolate the PSD circuitry from the subsequent circuitry and, therefore, avoid interference from next stage circuits.

Through the pre-amplification, the weak signals are amplified and then enter the operational amplifier circuits to implement arithmetic functions. According to the related principles, the subtraction signal $\Delta I = I1 - I2$ and the addition signal $\Sigma I = I1 + I2$ are obtained.

### 4.2.3 LASER PULSE-DRIVER TECHNIQUE

In the practical measurement environment, the background or ambient lights will seriously influence the measurement. The strong diffusive lights from surrounding area may merge the signal, or seriously disturb the signal that is to be detected.

Two approaches are employed to cut down such kind of interference. The first one is to simply envelop the PSD and the image lens in a sealed dark box. Therefore, the direct ambient lights emitting on the PSD are isolated and only the lights entering the lens can focus on the PSD, most of which are from the beam spot. The second method is to use the pulse-driven technique, through which the laser source is pulsed on and off at a fixed rate (set to 175kHz). As the laser beam is "off", the background lights fall on the PSD through the image lens. When the laser beam is "on", the combination of the signal and background lights project on the PSD.

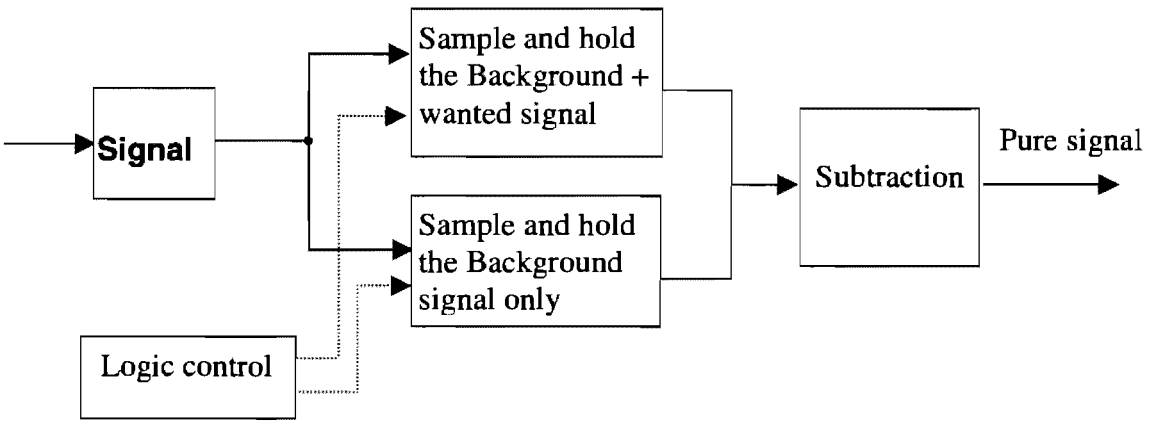


Figure 4.3 Block diagram of laser pulse-driver.

The operational circuit extracts the pure signal by subtracting the background signals from the combination signal. Figure 4.3 and Figure 4.4 illustrate the principle of pulse-driver.

### 4.2.4 PID CONTROL THE POWER OUTPUT

The reflectivity change is in a great variety of ranges with different material surface. For example, the reflectivity of the absolute black surface is 3% while a white paper is over 93%. The reflectivity depends much on the material, texture and color.

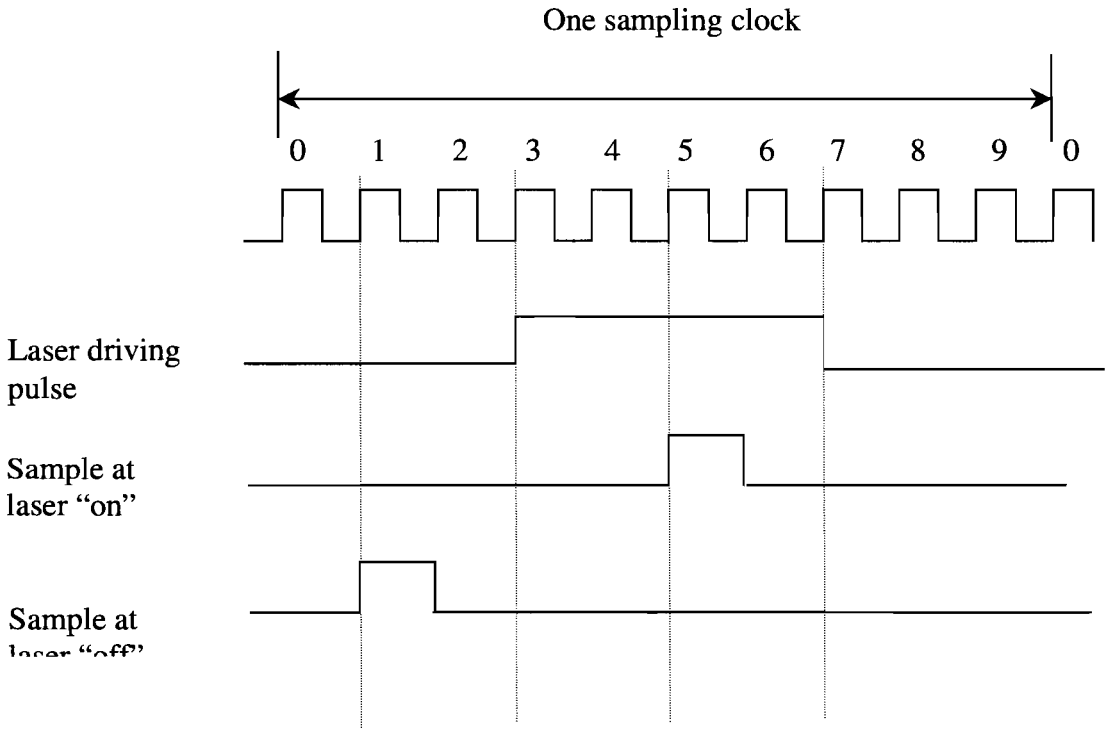


Figure 4.4 Timing diagram of laser pulse-driver.

This situation requires the output power of the system to adapt to this energy change, which means the control of the laser diode, should also have a wide dynamic scope. With a smooth surface target, the received light quantity is more than with a low-reflective target. The PID auto-gain automatically adjusts the gain ability loop according to the quantity of the received light. This function enables the measurement independent of the light reflective characteristic of the target, and gets stable.

Most lasers on the commercial market are Automatic Current Control (ACC) and Automatic Power Control (APC). They are not suitable for our application. A matched laser driver circuit needs to be developed for this study.

#### 4.2.4.1 COMPENSATION FOR THE REFLECTIVITY CHANGE

The color and texture of the pavement surface changes frequently while the vehicle runs on the road. The reflectivity varies at different sampling sites. The light intensity reflected on the PSD fluctuates during measurements.

From the theoretical analysis in Chapter 3, Equation (3.12) shows that the position information only depends on the spot's position on the PSD. The intensity of the light spot projected on the PSD does not determine the position. If the evenly distributed light is changed on its intensity, the output result is offset in the division calculation.

However, in the actual application, the intensity of the incident light does produce a bigger impact to the position measurement. The major reason is that the light spot is not an infinite small one, and the intensity of the light inside the spot is not evenly distributed. Even though the outline of the spot looks unmoved, the subtle texture of the surface causes the shift of the spotted centroid. This shift of the centroid results in error measurement. The experiments show that the error is too big to be ignored. For

example, conduct the experiments on different points at the same height level, the results show those points are on different heights.

The key point of solving the above problem is to keep the intensity constant, in another word, to keep the addition signal $\Sigma I$, expressed in Equation (3.12), as a constant. It can be realized by adding a negative loop, PID control loop, to the circuitry to regulate the output of the light, and then control the intensity of the incident light on the PSD. Using this method, the surface reflectivity changes are fully compensated.

Considering the wide dynamic range of the reflectivity, a 70mW laser diode is chosen for the system. The PID automatically adjusts the output power of the laser diode to times of the normal level to compensate the measurement errors caused by colour differences and angled/rough surfaces.

#### 4.2.4.2 ACCURATE COMPENSATION PROBLEM

When conducting experiments on a different color surface, slight differences are observed on the feedback signals $\Sigma I$, which are the input signals to control the power output of the laser. These slight differences indicate that the PID is not functioning satisfactorily.

After studying the voltage values of $\Sigma I$ against different surface color sent to the input of operational amplifier OPA548 (Figure 4.5), errors are found to be caused by the large values of the resistors *R27* and *R34*, which reduce the sensitivity of the circuit to the slight change of signals.

The original values of *R27* and *R34* in circuits are 5k and 3k, respectively. The value of signal $\Sigma I$ is set to 5.240V. From the experiments, the following results are obtained. See Table 4.1.

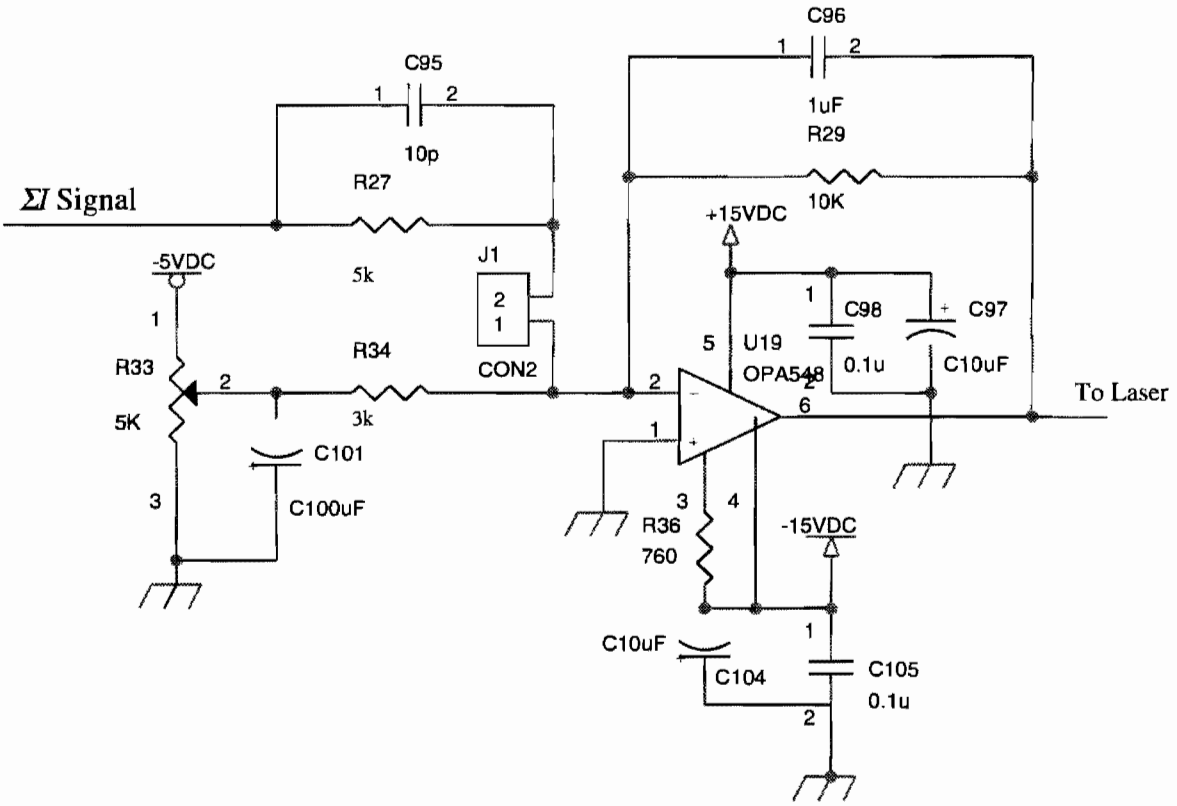


Figure 4.5 PID control circuits.

Table 4.1 Different voltage values at the input of OPA548 before changing the resistors

| Material surface color | $\Sigma I$ signal detected (V) | PID output Control signal (V) | Difference with the desired voltage (V) |
|---|---|---|---|
| White | 5.264 | 7.49 | -0.024 |
| Khaki (concrete color) | 5.237 | 8.01 | 0.003 |
| Dark gray (asphalt) | 5.202 | 8.60 | 0.038 |

From the above table, it can be seen that there are some errors between the targeted voltage 5.240V and the actual PID output control voltages. The signal $\Sigma I$ is not accurately close to the fixed input signal 5.240V – they are either higher or lower. This voltage difference affects the accuracy of measurements and leads to that the additional signal $\Sigma I$ can not be kept constant. This slight difference will cause the loss of the standard of the subtraction signal $\Delta I$.

From OPA548 pin-2, there are no changes detected against different colour. Thus, we can assume that the resistor *R27* and *R34* may affect the subtle voltage level at the input of OPA548. The small current does not demonstrate enough power to close the slight difference. The accuracy of PID control will be improved by adjusting the values of *R27* and *R34*. Table 4.2 lists the results after the adjustment.

Table 4.2 Different voltage values at the input of OPA548 after changing the resistors

| Material surface color for experiments | Summation signal detected (V) | PID output control signal (V) | Difference with the required voltage (V) |
|---|---|---|---|
| White | 5.264 | 7.49 | 0.000 |
| Khaki (concrete color) | 5.261 | 8.03 | 0.003 |
| Dark gray (asphalt) | 5.258 | 8.69 | 0.006 |

Comparison with Tables 4.1 and 4.2 shows that the differences have been greatly reduced to 1/10 on the average. However, the difference can not be completely eliminated due to the noise level in the circuit. The values of the resistor *R27* and *R34* need to be carefully chosen. Because a negative voltage will appear on the PID output if the input of pin-2 of OPA548 is a small positive signal and the ratio of *R27* to *R34* is less than 2.3, the oscillation phenomena may take place if the values of *R27* and *R34* are too small. The compromise values of *R27* and *R34* are 3.0kΩ and 1.3kΩ, respectively.

### 4.2.5 SAMPLE/HOLD AND SWITCHING TECHNOLOGY

After the signal passes the first stage, the sample/hold and operational amplifier, the signal gets rid of the background. At this point, however, another problem is introduced. As the sample/hold IC works in the sampling mode, the peak (or valley) appears in the signal (Figure 4.6). This uncertain phenomenon is caused by the charge leak of the internal capacitors. A serious problem will be incurred while this signal is sent to the PID control input.

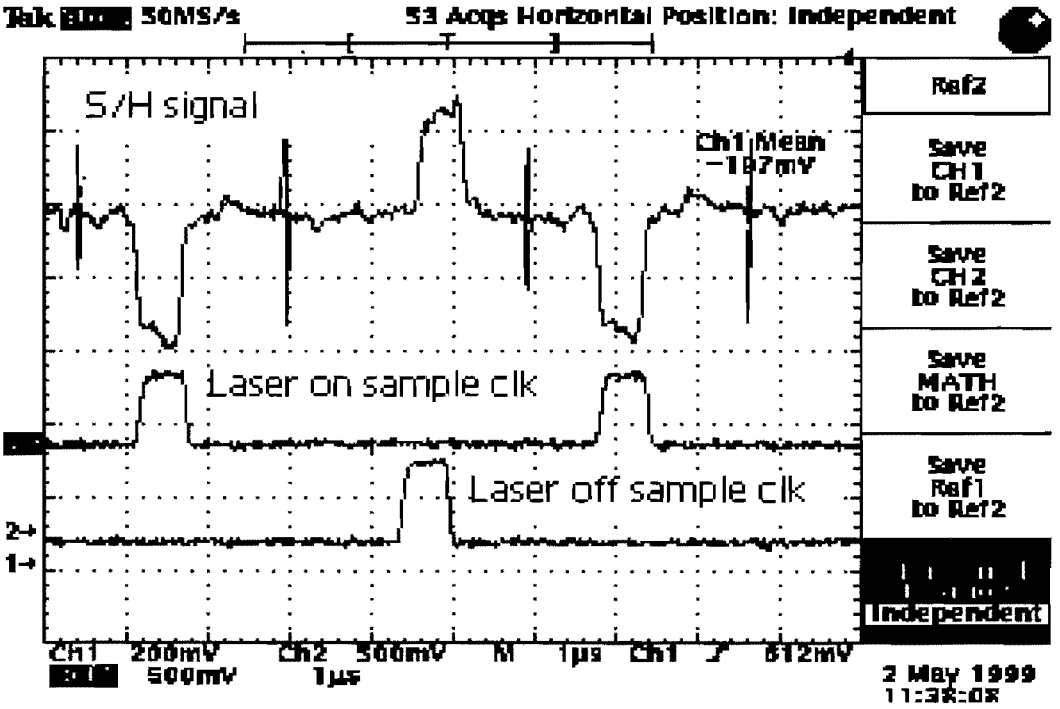


Figure 4.6(a) Peaks and valleys in the signal.

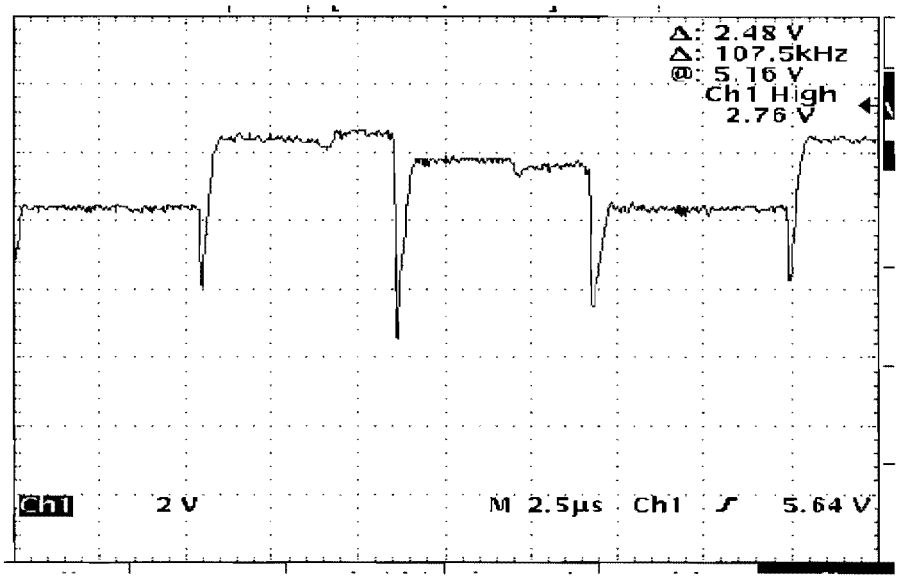


Figure 4.6(b) Oscillation at the control output sent to the laser driving circuits.

At early time, an integral capacitor 1μF (*C96* in Figure 4.5) was used to absorb these droops and towers in signal (the feedback resistor *R29* = 10k). The control speed of the PID loop was seriously slowed down. The response time to the 1.0V change takes a long time --1ms~2ms.

As shown in Figure 4.7, a very slow climbing phenomenon is observed. The measurement error in the profiling is due to the slow PID control speed. Some approaches were experimented to improve the input signal. For example, the high-speed sample/hold is tested to see if a narrow droop could be found and the DC restoration chip is used to see if the DC voltage level of the signal could be retrieved. After the comparison, an optimal method was found, which is to employ the analog switch to alternate the signals held by the sample/hold chips. Figure 4.8 is the flow chart to illustrate this approach.

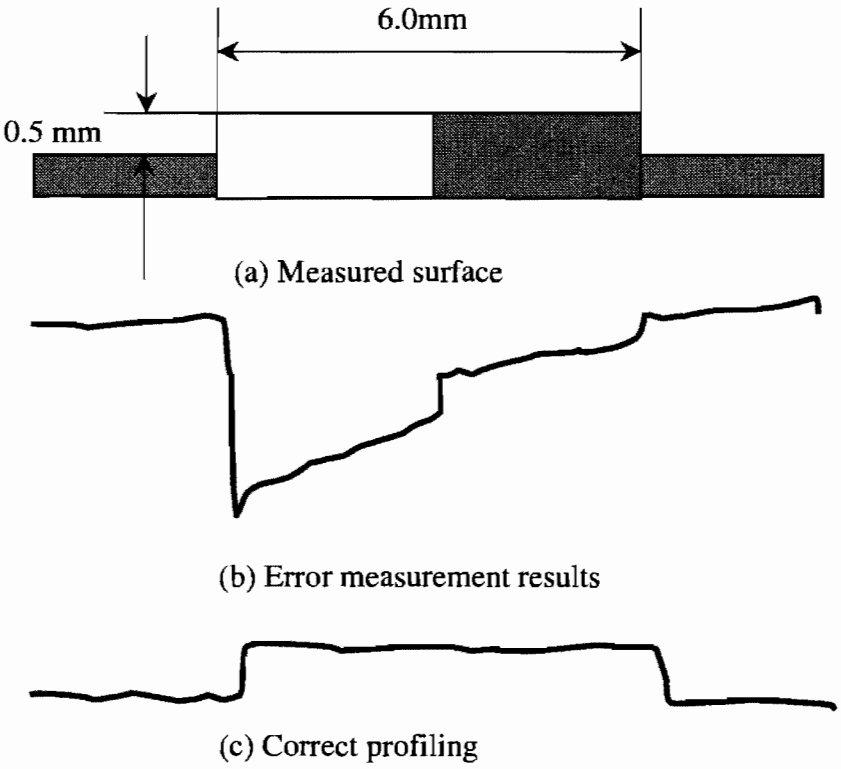


Figure 4.7 Measurement on the colored surface.

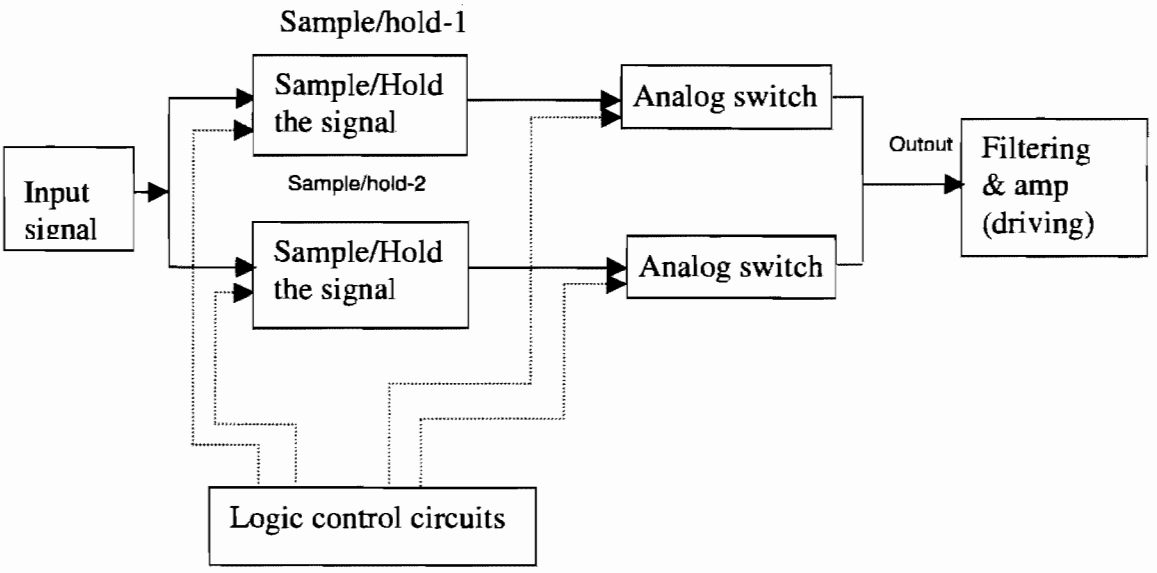


Figure 4.8 Sample/hold switching approach.

When sample/hold-1 is in sample mode, switch 1 is turned off. At this time, sample/hold-2 is in hold mode and holds the signal. Switch 2 is on and passes the signal to output. While the sample/hold-2 works in sample mode, droops appear and switch 2 is off. In the mean time, sample/hold-1 is in hold mode and holds the signal that is to be sent to output. Switch 1 is on, letting the signal pass. The output then obtains the stable signal that is switched from sample/hold-1.

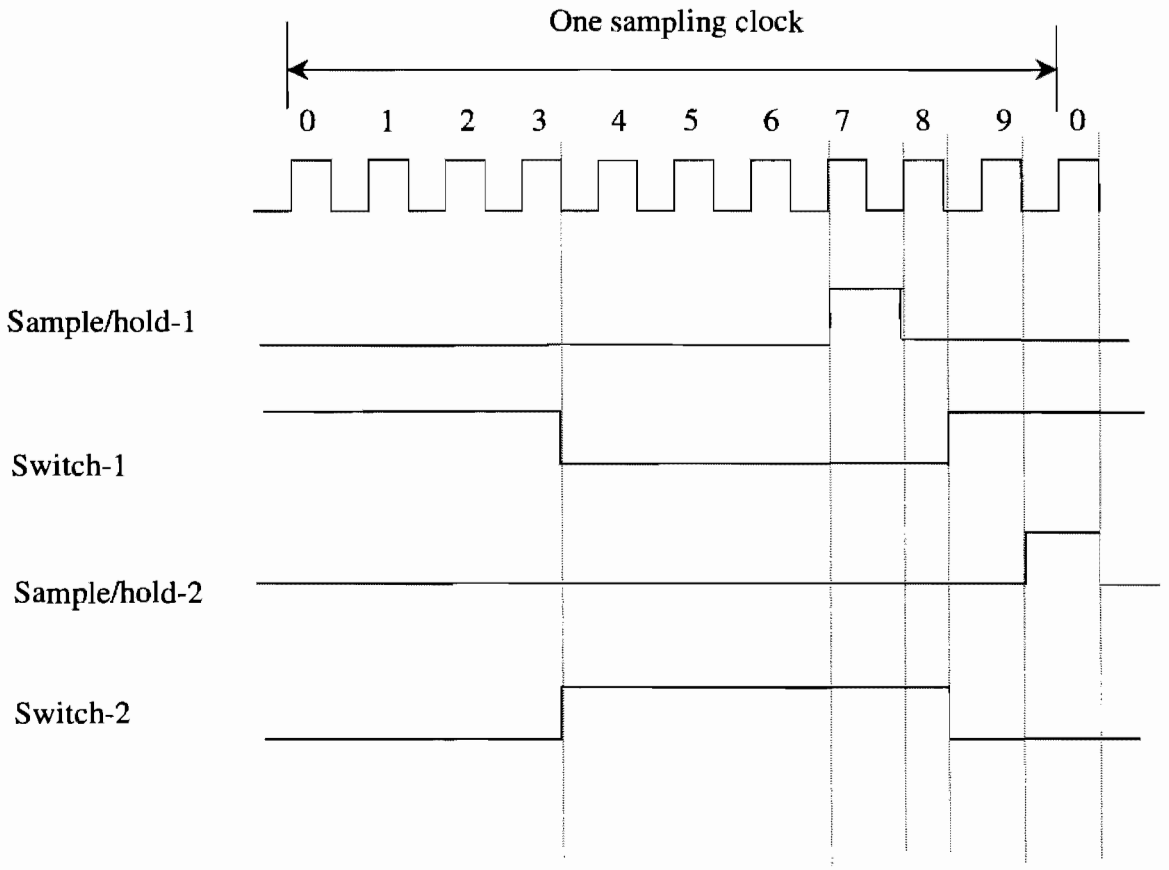


Figure 4.9 Timing Diagram of Sample/Hold and Switching.

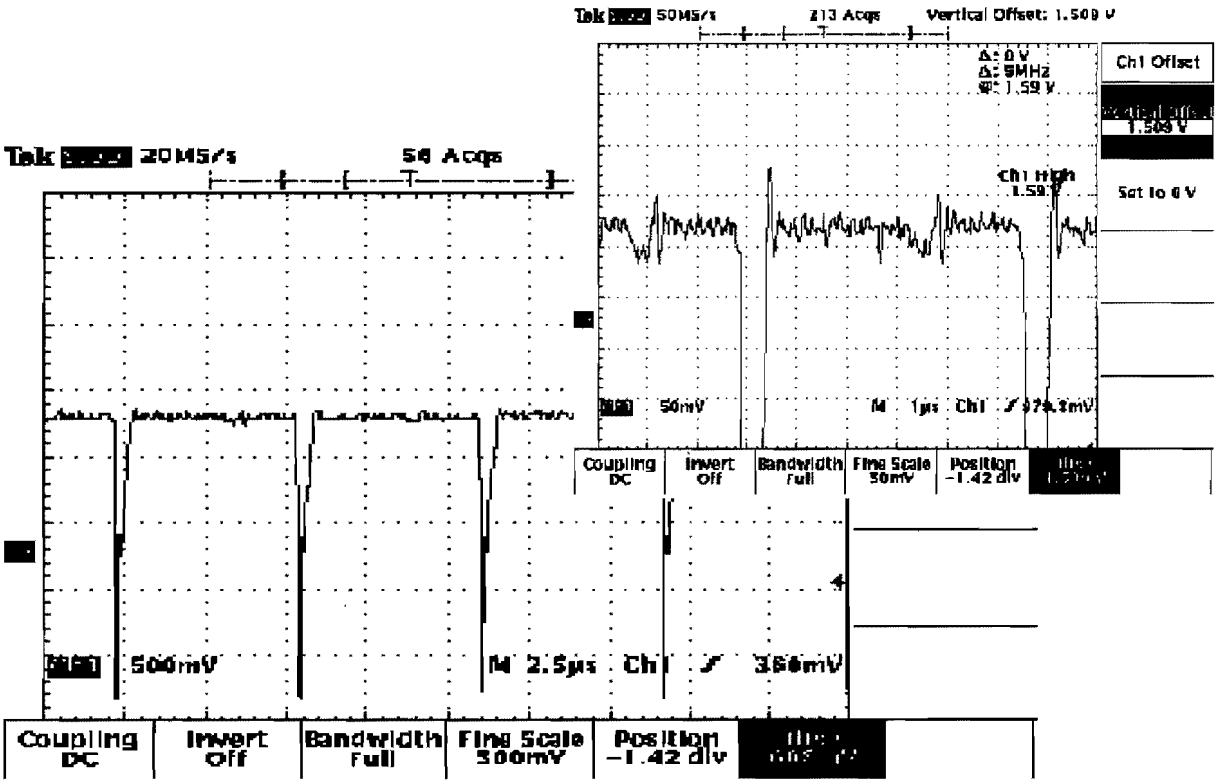


Figure 4.10 Signal distorted with droops

The droops or towers are caused by the leakage in the sample/hold internal capacitors. Because one output of the sample/hold is connected to the ground through the resistors, the leak causes the voltage dropping sharply.

Figure 4.11 shows the signal output from the switches. After the switches, the big droops are basically removed. However, the small spike noise, generated by the digital circuits, still exists.

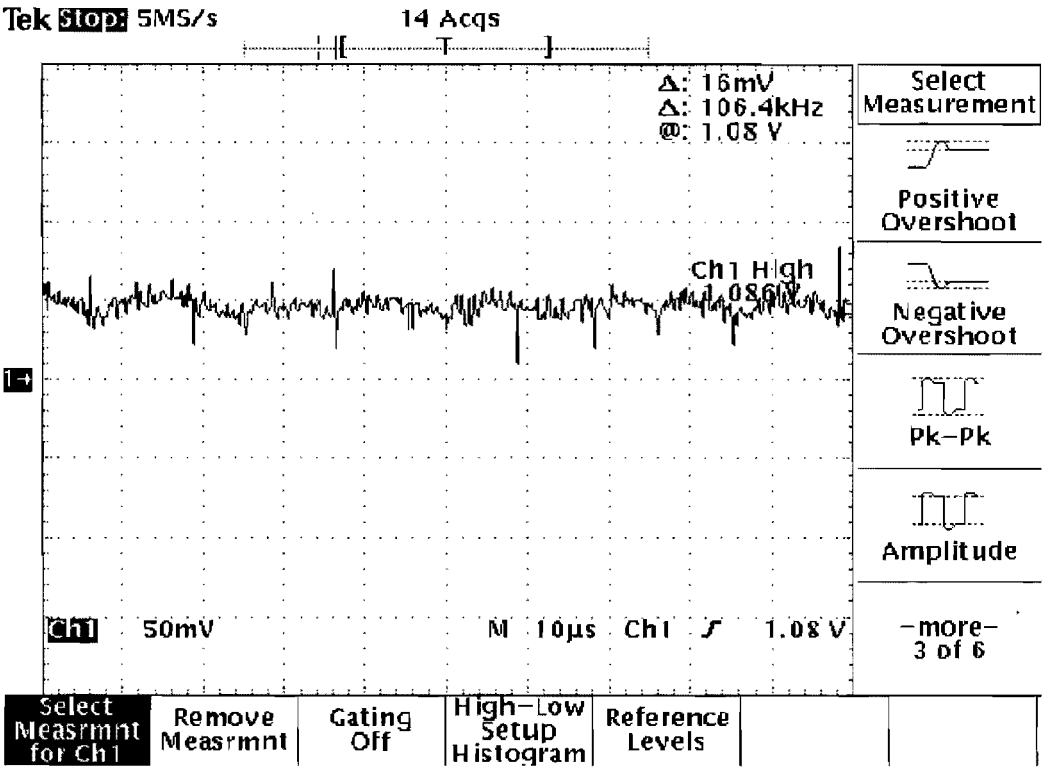


Figure 4.11 Signal after the sample/hod and switching.
Note that the system conversion is 8 µm/mv.

### 4.2.6 FILTERING APPROACHES

The noises always exist in analog circuits, such as the thermal noise and white noise. The digital circuits also introduce strong interference to the analog circuits. Using low noise components, such as the high precision resistors and low noise chips, may reduce the system noise. In the application circuits of the operational amplifier, a good balance may also alleviate the noise. For example, in the basic circuit connection, the accurate and matched resistors and capacitors can help the op-amp to lower the noise level.

Other than the above methods, two filtering techniques are employed in circuits as well. The first method is to use a capacitor to change the rectangular shape of the pulse that is fed for the pulse-driven. This method, in substance, is to change the differentiate coefficient of the pulse. The strong suddenly turned-on current by the transistor *Q1* introduces the spike in the circuits as shown in Figure 4.6. These interference affects all signals from the first input to the last output. The capacitor *C103* changes the pulse shape from the steep rising and dropping to gradual climbing shape. The capacitor *C103* almost completely removes the big spikes on the signals.

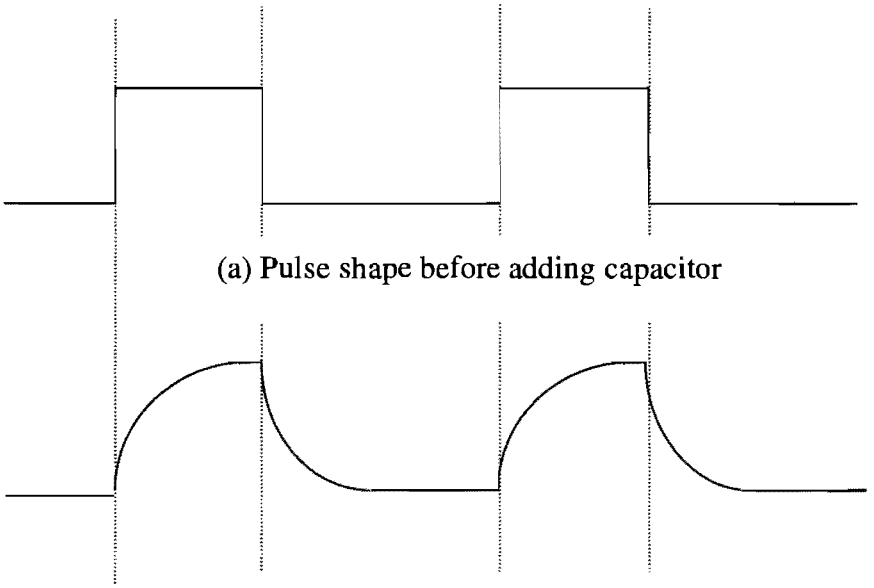

(a) Pulse shape before adding capacitor

(b) Pulse shape after adding capacitor

Figure 4.12 Capacitor changes the pulse shape.

The affection of the shape change is that the width of the pull-down pulse generated at point *V9* by *Q1* becomes narrow, while the shape still stands well. No affection is applied to the laser diode.

The second method is to use a first-order low pass filter. This is to remove the spike-liked noise left on signal as shown in Figure 4.10, which also comes from the

digital pulse. According to the Fourier transform analysis, the noise frequency is distributed above 500kHz, which is much higher than the system operation frequency 175kHz. Therefore, the first-order filter is employed, as a low pass filter, to let the signal, whose frequency is lower than 200kHz, pass the filter. Figure 4.13 is the filtered signal.

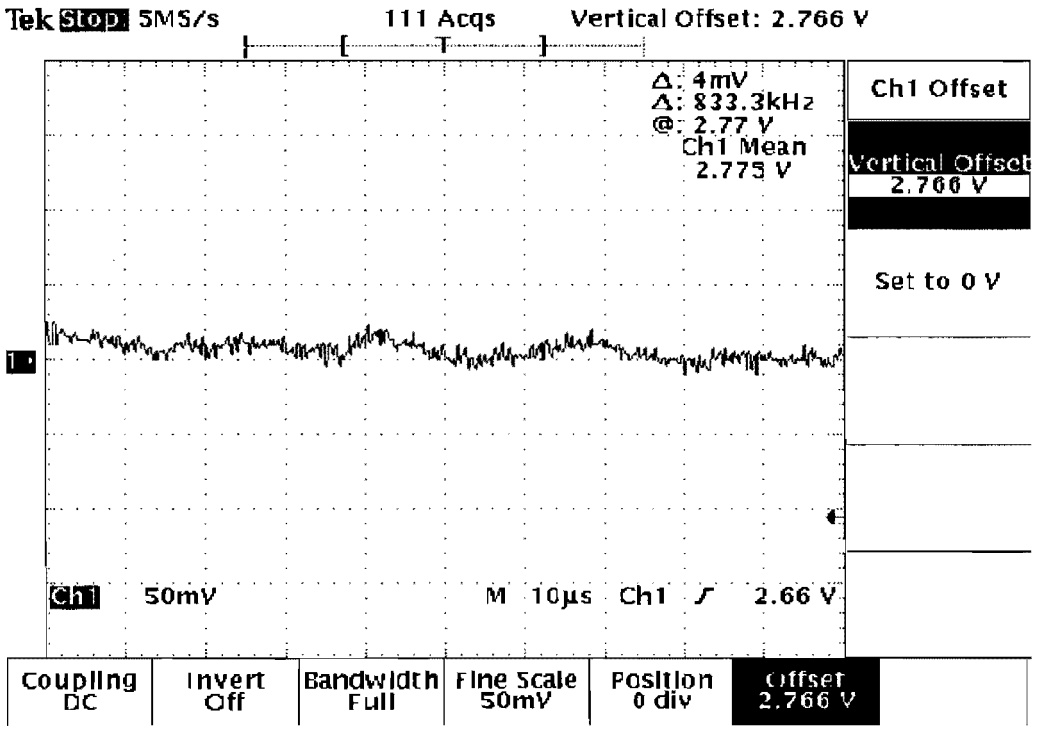


Figure 4.13 Signal finally obtained after passing the first-order Low-pass filter.

In order to have a higher voltage as the denominator in the division calculation, the filter is also designed as a 2.4 times amplifier. Thus, the $\Sigma I$ (addition signal) voltage reaches 2.60V, while the noise is curbed at the 50mV level, which is good enough to be used as the input signal of PID.

### 4.2.7 LOGIC CONTROL CIRCUIT

In the circuit design, the chip LMC555 (timer) is selected as the clock generator, which has a large adjustable frequency range from several hundred kHz to 4.0MHz. According to experiments, the frequency 1.75MHz is chosen as the basic clock, through which the laser pulse rate 175kHz is obtained. Other control logic signals, such as the sample/hold mode control of the light-on and light-off, synchronization of the control sequence for the sampling and switching, and the interface of the sampling trigger, are all generated. Figures 4.4 and 4.9 explicitly illustrate the logic timing of the control signals.

### 4.2.8 LASER DRIVER AND PROTECTION CIRCUITS

A common circuit for the laser diode driving in low power applications adopts APC and ACC. The constant output power and operation current are required in these applications. The feedback control loop is utilized to keep the operation under the constant conditions. The switching regulators, such as *RC4190*, which can provide DC to DC conversion by internal step-up or step-down circuits, are the typically used components in the implementations.

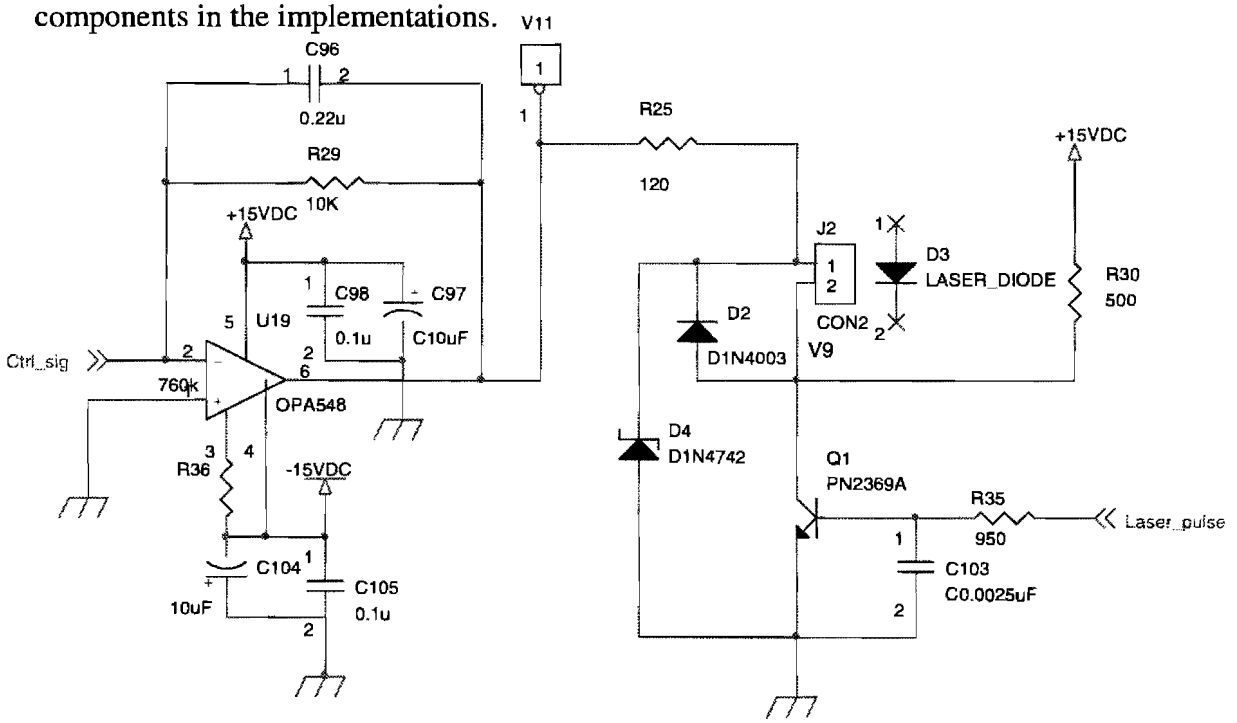


Figure 4.14 Laser driver and protection circuits.

In this study, the measurement is usually conducted in the environment with the fluctuated reflectivity. The APC and ACC are apparently not suitable for this situation. PID control requires the output power could be frequently controlled by the reflected intensity. The control is achieved by adjusting the output voltage applied on the laser diode. The input signal ($\Sigma I$ signal) determines the amplitude of the output voltage. In Figure 4.14, the OPA548 (high current operational amplifier) regulates the amplitude of the voltage applied on the laser diode *D3*. The pulse signal controls the switch transistor *Q1*, which lets the laser diode operate under the pulse frequency of 175kHz.

Figure 4.15 (a) is the voltage amplitude at point V11, the positive end of the laser diode. Figure 4.15 (b) is the voltage amplitude at point V9, the negative end of laser diode. The voltage amplitude and pulse signals are combined according to this circuitry.

The pull-up resistor *R30* is used to improve the voltage shape at point *V9*, letting point *V9* have a higher cut-off voltage to turn-off the laser diode when transistor *Q1* is in turn-off status.

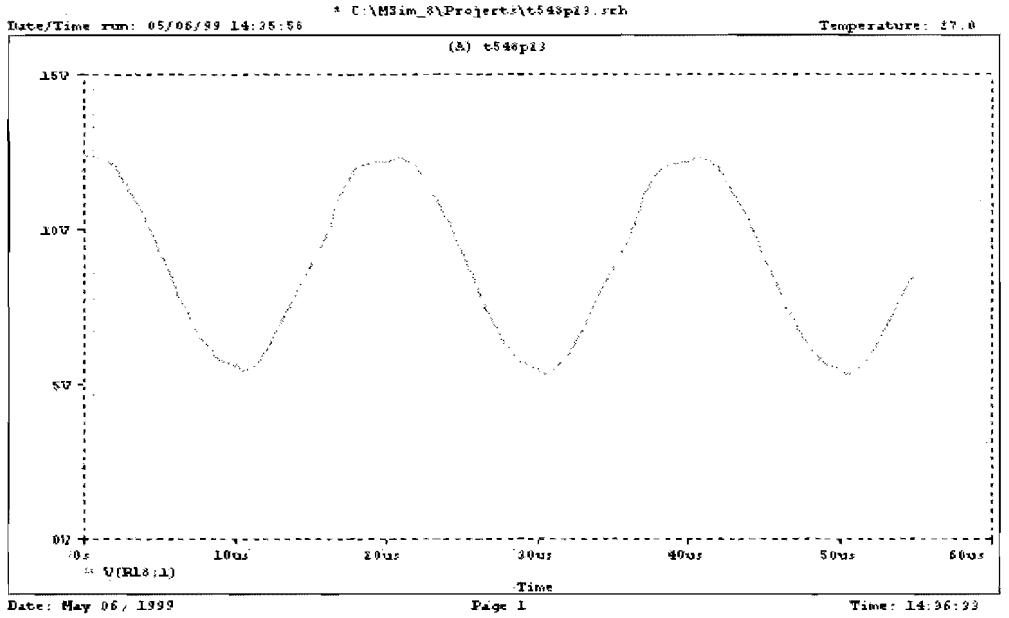


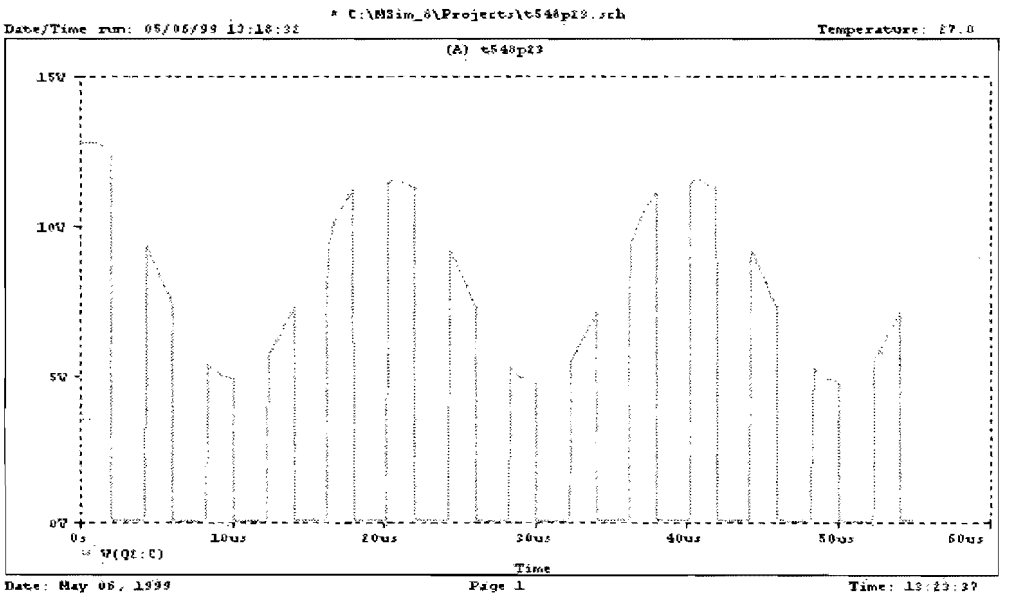


Figure 4.15 Voltage waveform at point V11, which is applied on the positive pin of the laser diode (Pspice simulation).

The protection is implemented in two aspects. The first one is on the voltage. Zener diode *D4 4742* is used to limit the voltage. Any voltage higher than 13.60V is regulated by *D4* and the extra current leaks to the ground in case a higher voltage is applied. The diode *D2* is adopted to avoid any reverse voltage added on the laser diode. The reverse voltage will be released once the negative voltage occurs at the point *V11* or the voltage at point *V9* is higher than point *V11*.

The second aspect is the current protection. Despite the type of the circuit, the driven current of laser diode must not overshoot the maximum operating level; even a nanosecond will damage the mirror coatings on the end facets of the laser diode. *R25* is used to limit the current that flows through the laser diode. Another resistor *R36* is added to fix the output current of OPA548. The maximum current allowed to output is 95mA. The normal operational current of the laser diode *DL7140* (70mW) is 100mA (maximum 140mA at 25°C). Considering the spikes, surges, and other switching transients in the circuit, especially at the time of the electricity turned-on, a 30% below the maximum current value is chosen as the operation current for the laser diode *DL7140*. The heat-release factor should be taken into account. A 120Ω, 1W power resistor is chosen for resistor *R25*. Experiments indicate that the resistance of the laser diode is dynamic, varying from 20Ω to 60Ω. The proper value of *R25* guarantees the normal operation of the laser diode and the measurement system.

### 4.2.9 POWER SUPPLY PROBLEM

Any caution is necessary due to the use of digital and analog circuits in the design. Some IC chips accommodate digital and analog signals at the same time. The grounding problem must be handled very carefully. While routing the circuits, the digital ground and the analog ground should be separated and be connected at one point only. It is better to choose the joint point at the input connection port.

To avoid spikes and surges on the power supply, capacitors with values of 0.1μF and 10 μF should be put beside each IC chip. For the general power supply, 470μF capacitors are employed to provide a more stable voltage.

## 4.3 DATA ACQUISITION INTERFACE

The data acquisition interface consists of two parts: hardware interface and software. The data acquisition board is a product of Data Translation Co. The maximum sampling rate is 333kHz, which matches the requirement of the sampling rate at 175kHz in the measurement system.

The software HP VEE provides an efficient and friendly interface between the user and the data acquisition board. End user has the right to decide the way of data acquisition, such as the control speed, the number of channel, and the data access style. Figure 4.16 gives an example of using the HP VEE in measurement.

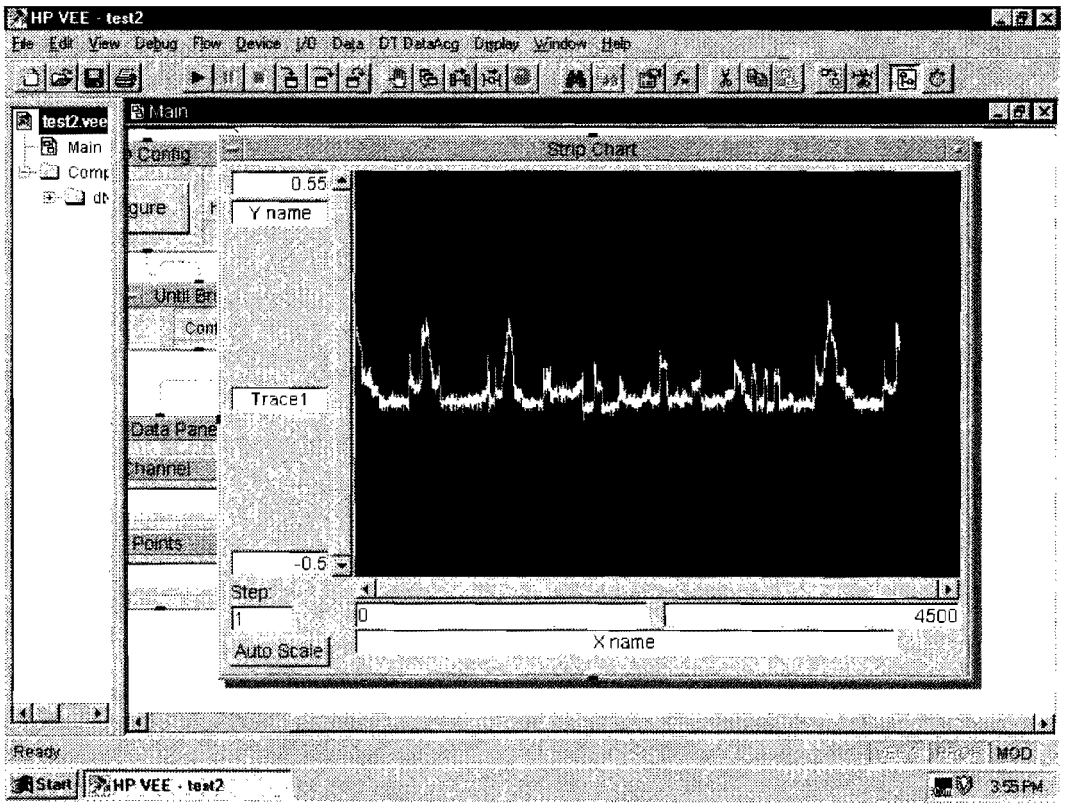


Figure 4.16 Data acquisition window.

# CHAPTER 5: LAB EXPERIMENT RESULTS AND ANALYSIS

## 5.1 GUIDELINES FOR EXPERIMENTS

The design purpose of the measurement system is to profile the texture structure of the pavement (highway) surface. All experiments should be designed to accommodate the various situations in the pavement measurement.

The macro/micro texture variation on the pavement surface demonstrates in two principal features: the angle variation of the facets, and the color change at different sites.

The experiments should simulate the actual measuring situations as closely as possible. For example, the tested surface should vary with shapes (angle) and colors (different materials). To define the major features of the measurement system, two critical parameters -- the fast sampling speed and the response time to the reflectivity change-- should be evaluated.

## 5.2 BASIC EXPERIMENTS

### 5.2.1 MEASUREMENT RANGE AND STANDOFF

Due to the electrical characteristics of the PSD and signal circuits, the standoff distance is set to 50.0mm. The spot image is focused on the PSD (position sensitive detector), which length is 34mm. The range of the corresponding measurement is 40mm. (The distance between the instrument box is from 30.00mm to 70.00mm.) Its effective measuring range is supposed to be 20mm.

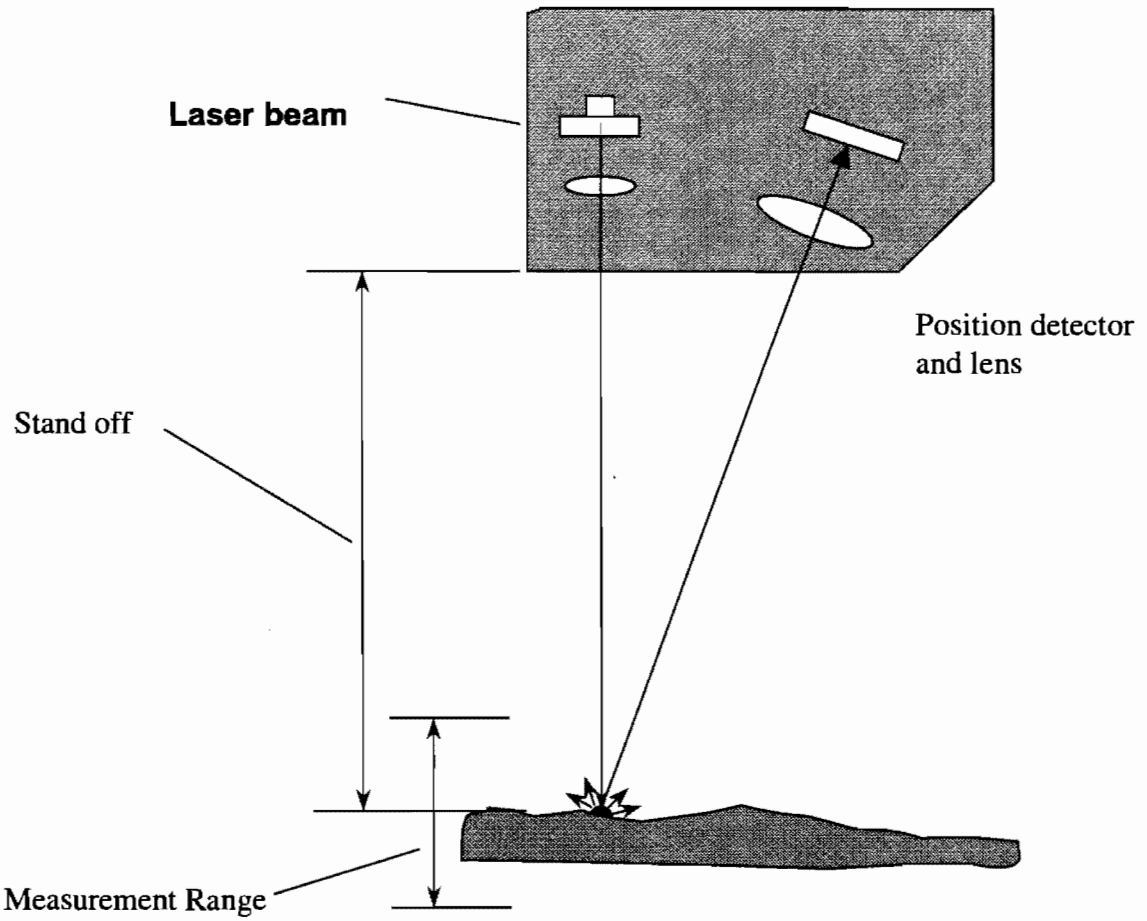


Figure 5.1 Measurement on pavement surface.

### 5.2.2 SCALING AND LINEARITY

This experiment is to find out the measurement scale -- the ratio of the voltage (position on PSD) to the actual height (position) variation. As object moves from 3.5mm to 6.00mm within the measurement range, the output voltage (position) changes from 1.679V to –1.777V. Calculating the 51 points, the approximate scale is about 0.069V/0.5mm = 138.24mV/mm.

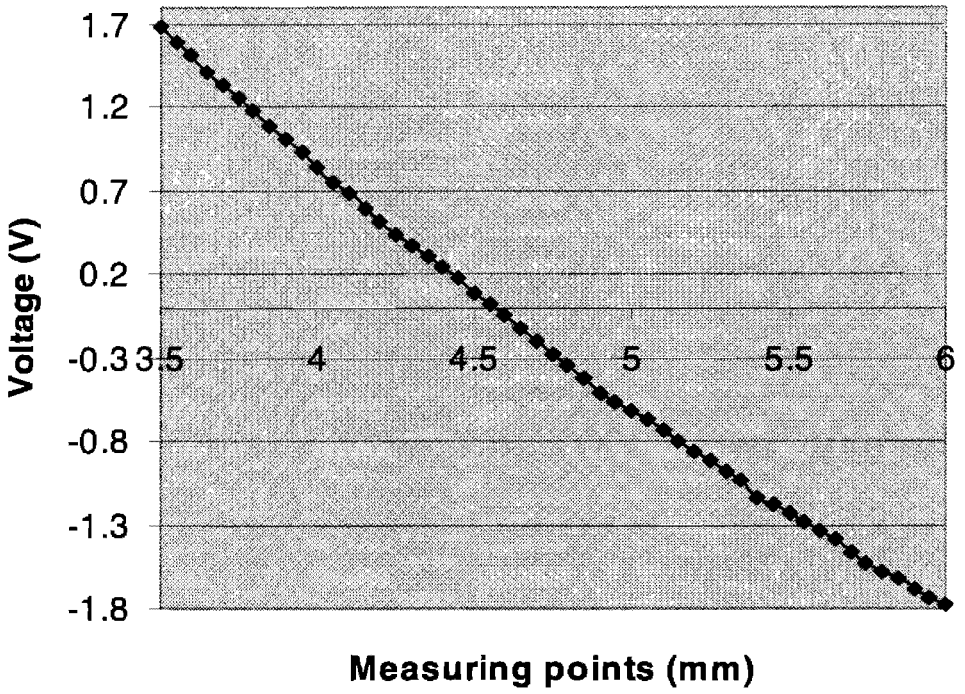


Figure 5.2 Scale and $H$ vs. $p$ curve

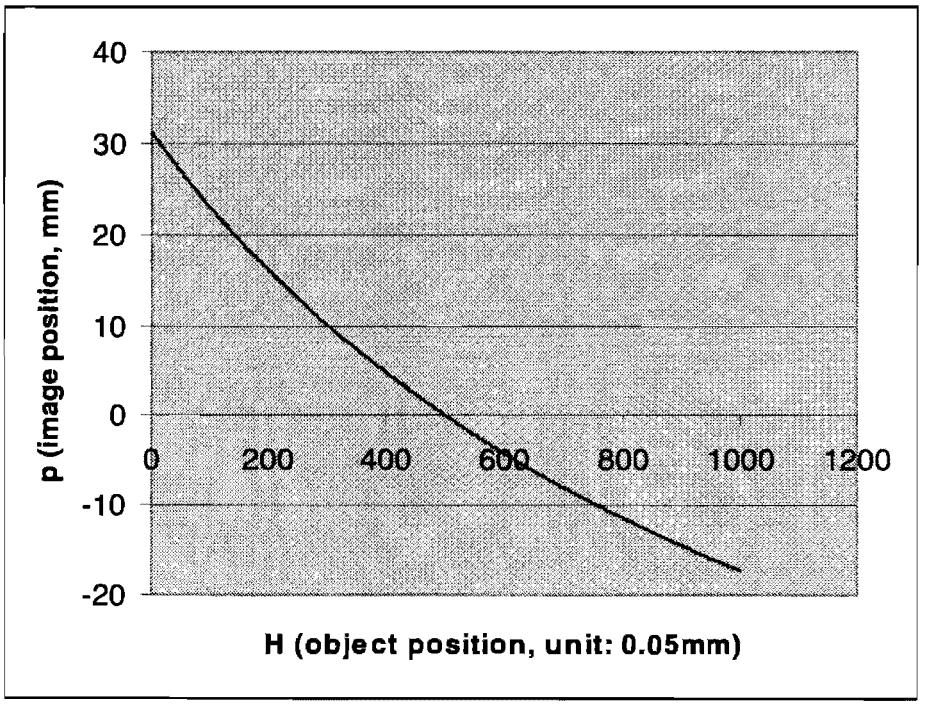


Figure 5.3 Curve calculated by Equation (3.10)

The relationship between the height (H) and the length of the image (p) on PSD can be calculated from Equation (3.10). Figure 5.3 is the theoretical curve. It is easily found that Figure 5.2 and Figure 5.3 are two equivalent curves. The data obtained from the measurement could be calibrated in data processing.

### 5.2.3 LEVEL OF NOISE

Like any other analog circuit application, the thermal noise and other interference exit in the circuits. There is also another source of noise, the opto-electronic components -- PSD.

To evaluate the accuracy, the noise level is the first factor to affect the accuracy of the measurement. From Figure 5.4, it can be seen that the maximum of the noise level is about 40mv and the constant noise level is 20mV.

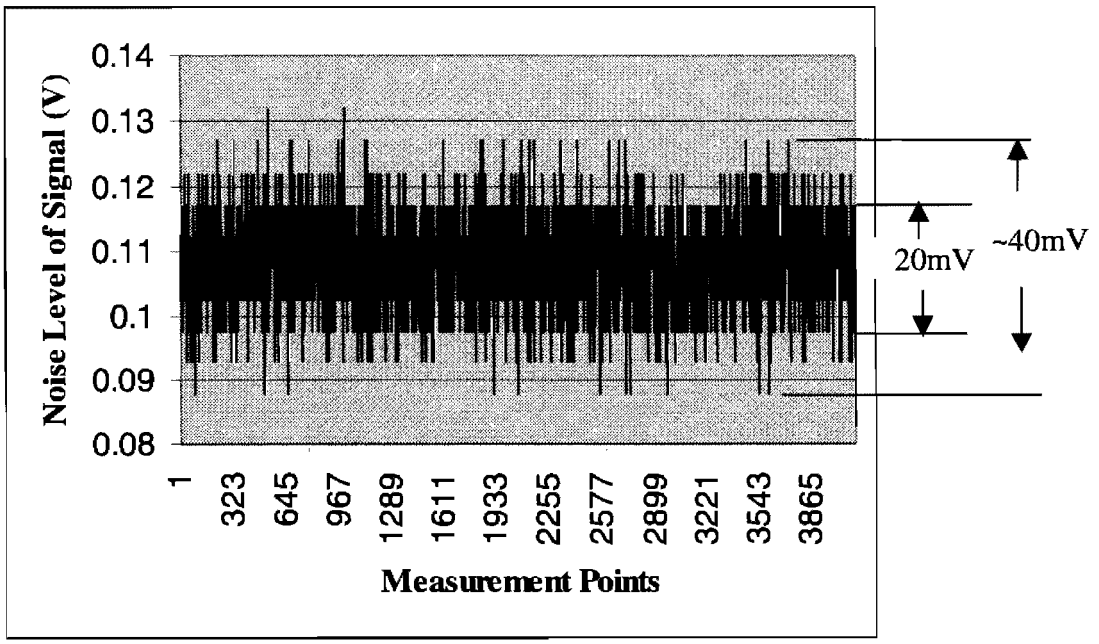


Figure 5.4 Noise level in signal.

### 5.2.4 ACCURACY (RESOLUTION)

The accuracy or resolution is a major parameter reflecting the measuring ability of the system.

In Figure 5.5(a), the interval of the measured points is 10μm. The four curves represents four group data. AVG1 is the curve of average value of 30 points, AVG2 the curve of average value of 50 points, AVG3 the curve of average value of 100 points and AVG4 the curve of average value of 200 points. It can be seen that AVG1 through AVG4 are almost the same. Therefore, if smoothing more points, the system accuracy would be 10μm.

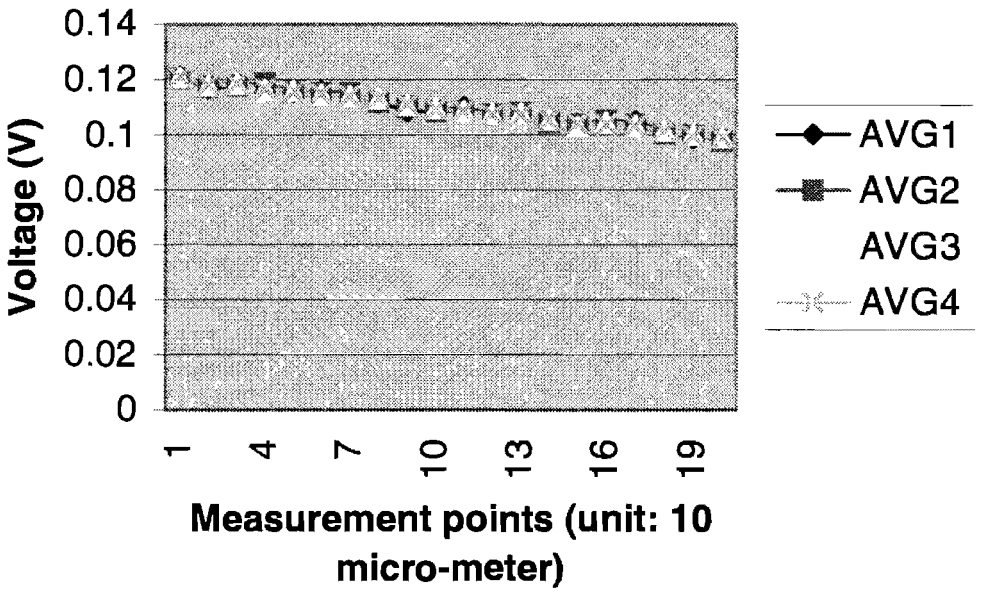


Figure 5.5(a) Static test with average

In Figure 5.5(b), the measurement distance is fixed at 5.0 cm. The voltage is the average of 1 sample point to 200 sample points.

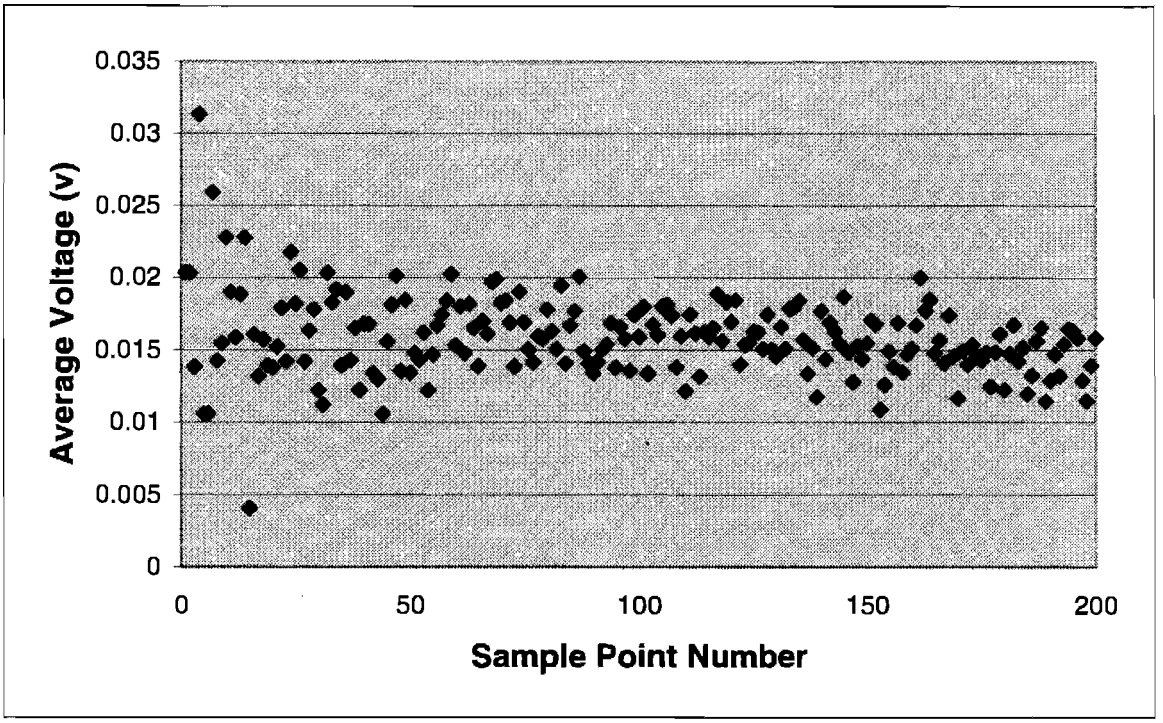


Figure 5.5(b) Static test with average

However, there is one point to be mentioned. The data acquisition board used in our system is 12-bit wide, which means its minimum resolution voltage is 10mV. If using a wider bit data acquisition board, the system resolution may reach a higher level. In dynamic measurement, the resolution becomes 100μm, which can be observed from Figure 5.7.

### 5.2.5 WARM-UP TIME

Figure 5.6 is the curve of the warm-up time. The circuit reaches stable state within 20 minutes. Output voltage change vs. temperature is also measured. For the temperature changes from $0^0$C to $50^0$C, the magnitude of the output voltage is about 15mV. The texture usage doesn't care about this drift. For the texture measurement slow drift is not a problem because we are only interested in fast change.

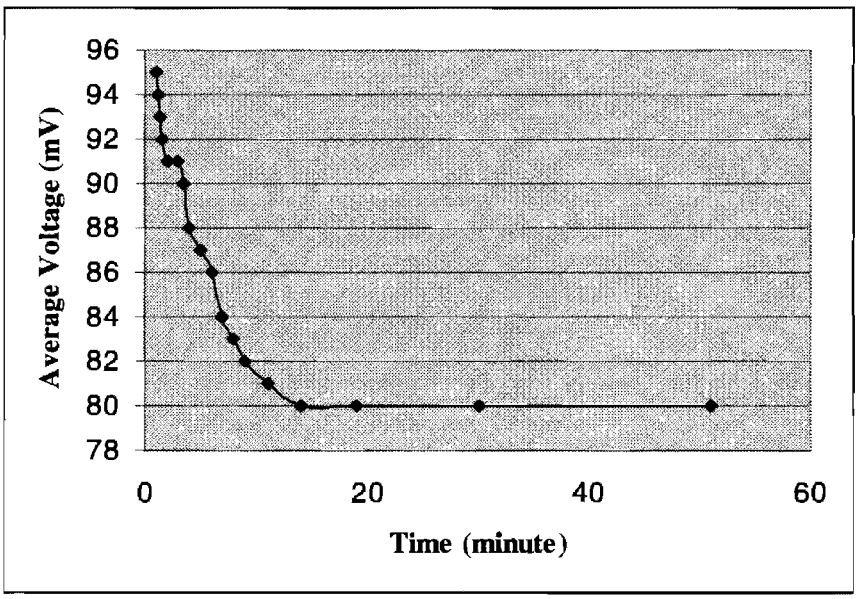


Figure 5.6 Stability characteristic of the sensor system

## 5.3 LAB TESTS

### 5.3.1 DIFFERENT SLOPE (SHAPE) AND HEIGHT OBJECT MEASUREMENT

In Figure 5.7, three rectangular shape surfaces are painted as the concrete color. The measurement is conducted on the surface of a moving object at the speed of 8.6m/s. The texture of the surface is correctly recorded. The height of the shape is 0.56mm. From the figure, the curve has precisely drawn out the texture of the surface. The noise level is about 100μm.

The spike that shown on the right side of the protruding shape is the measurement error caused by the blocking of the reflected light, which leads the addition of the signal to reduce sharply.

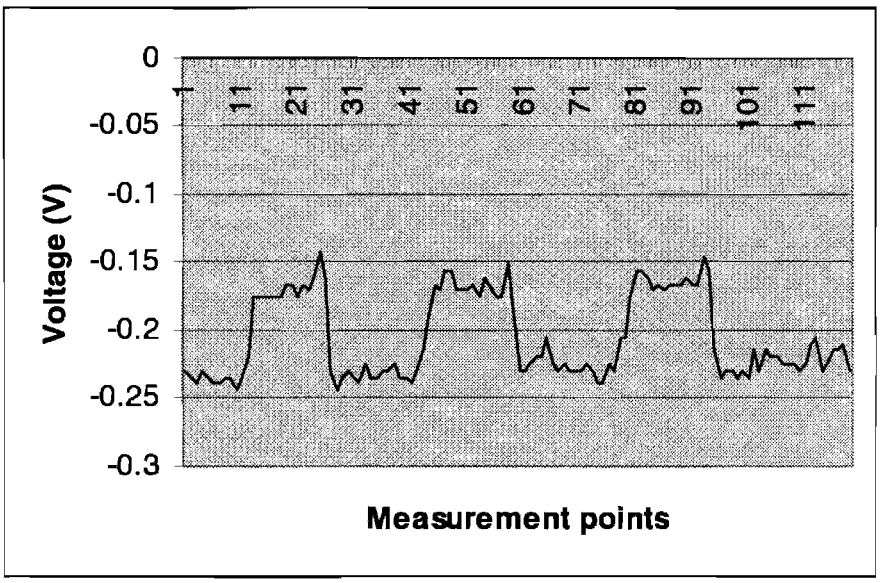


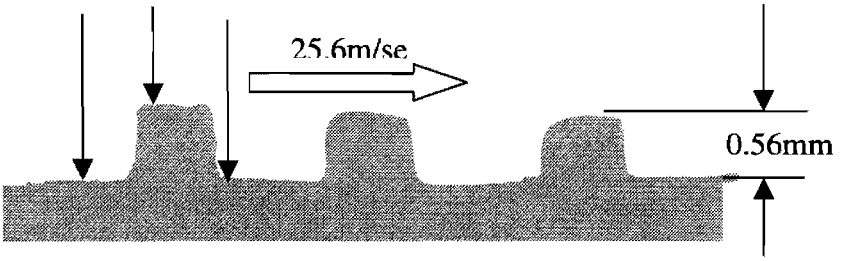


Figure 5.7 Measurements on three 0.56mm heights.

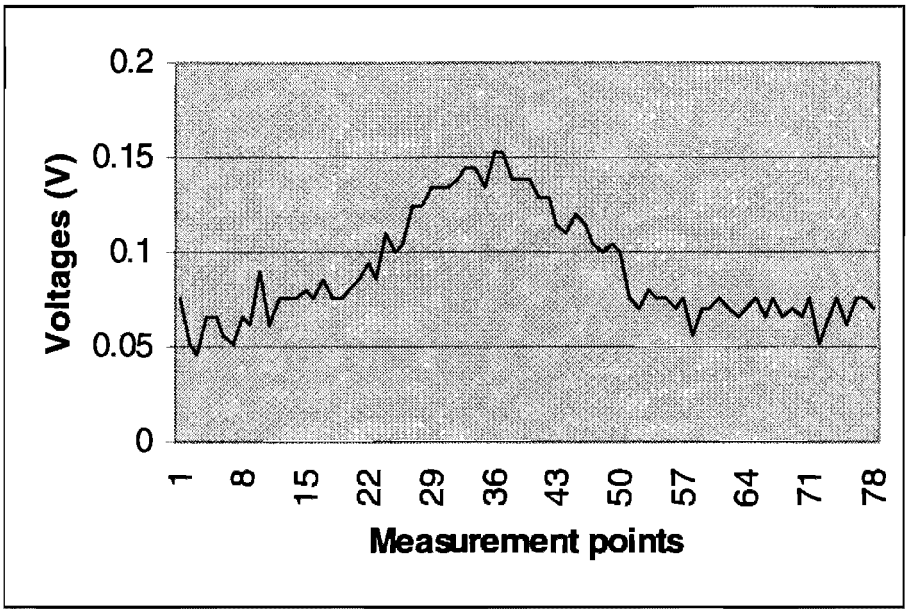


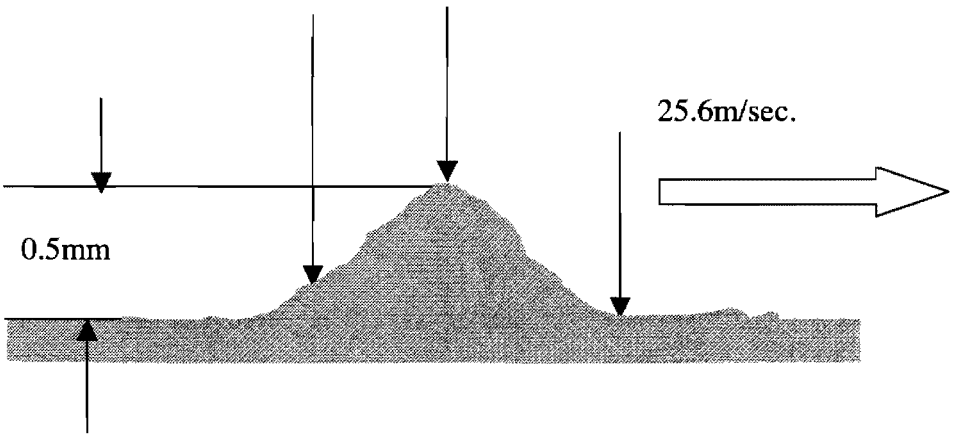


Figure 5.8 Angled shape surface.

The angled shape (or slope surface) is the frequently encountered situations in actual measurement. This profile curve indicated that the measurement profiling matches the actual shape of the object surface.

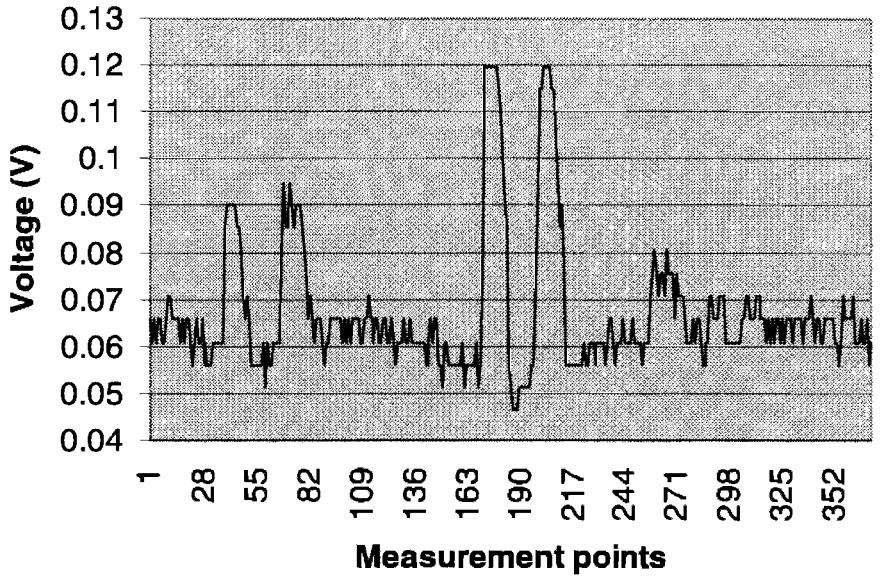


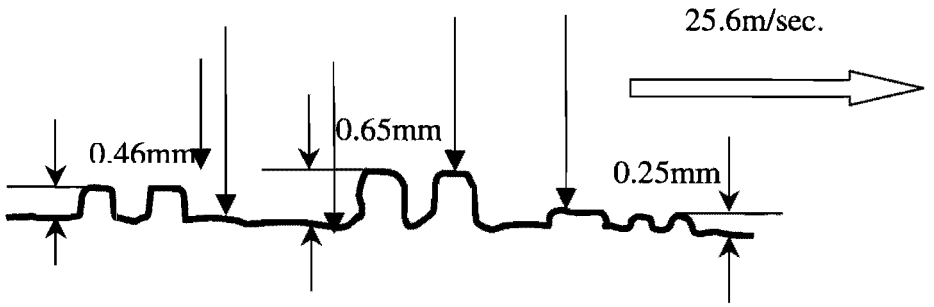


Figure 5.9 Measurement on different height surface.

This experiment in Figure 5.8 is conducted on a moving object running at the speed of 25.6m/sec (60mile/hour), aiming to check if the system is effective on the tiny things. The results show that the surface with the height of 0.25mm is distinguishable. Figure 5.9 shows a similar test with different hight.

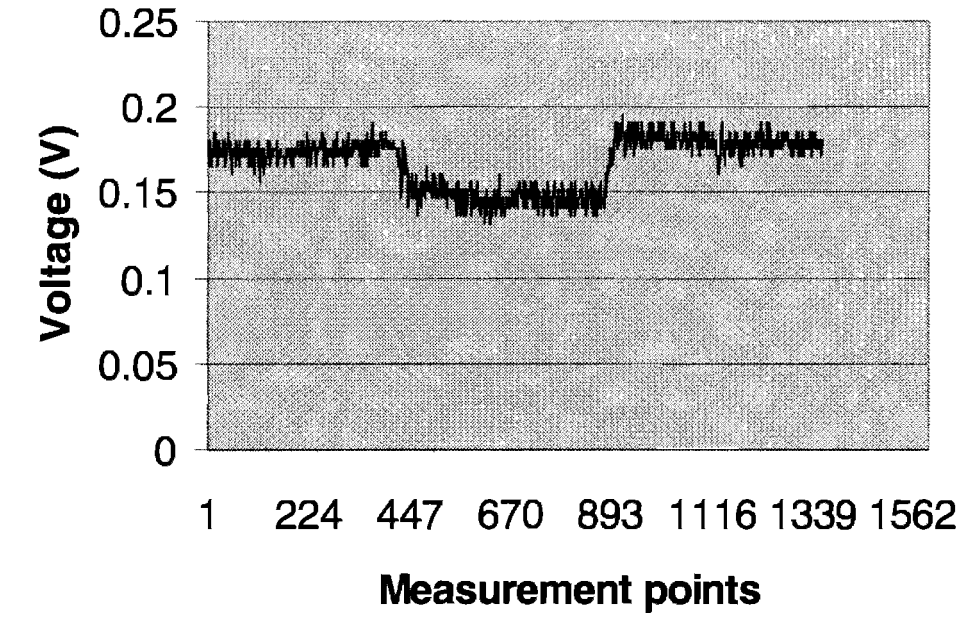



Figure 5.10 Color change at same height level.

### 5.3.2 COLOR SENSITIVITY TEST

Figure 5.10 illustrates the system's correct response to the color change on the same height surface. The color change from red to white causes the voltage on the PID input signal a 0.5V jump. With this burst signal change, the system works well. The correct and prompt response to the sharp variation is then realized.

### 5.3.3 DIFFERENT COLOR AND DIFFERENT HEIGHT

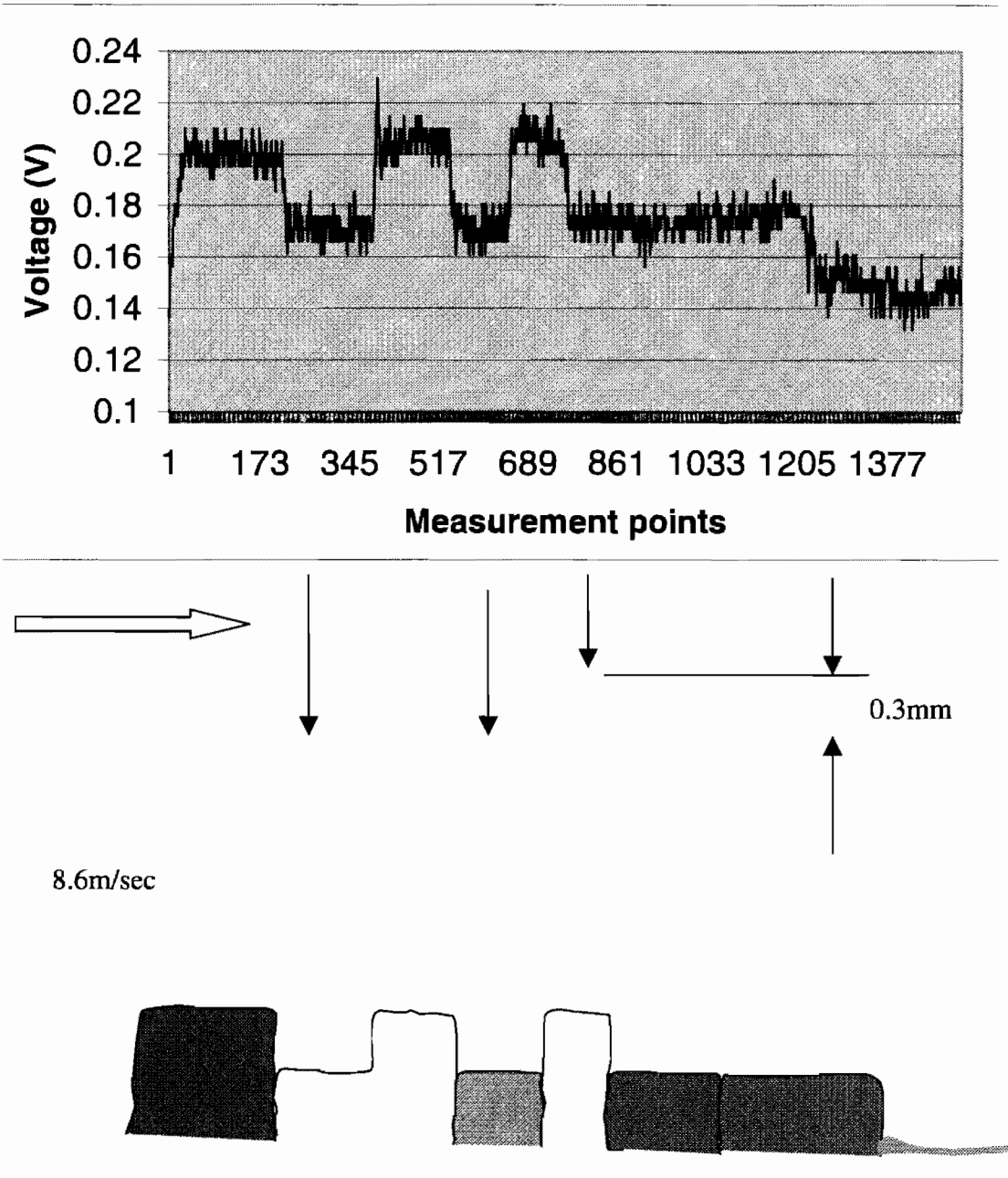


Figure 5.11 Response to different heights with different colored surfaces

In Figure 5.11, although the color and height have all suddenly changed, the curve is still obtained correctly. Figure 5.12 shows the angled shape and color change situation.

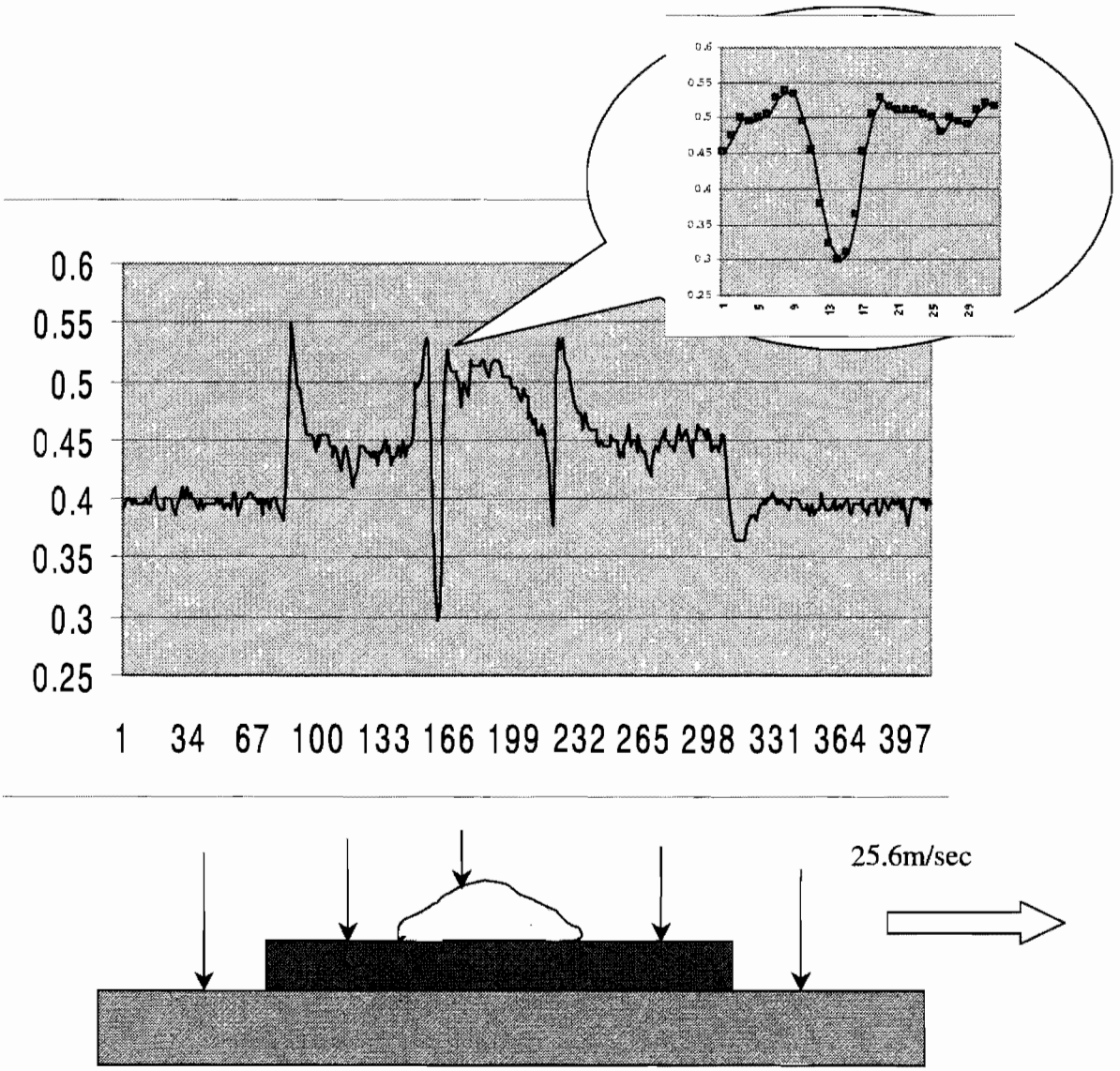


Figure 5.12 Varying slope and sudden color change.

The sudden color change causes the steep jump of the control voltage. Some time

is needed for the system to adjust to the new state. In Figure 5.12, the time of the transient period for 21 points to the new state is 25×5.6μs = 140.0μs, which is 7.1kHz.

### 5.3.4 IMPACT OF THE STRONG AMBIENT LIGHT

If put the system under different ambient light environments--for example, by illuminating the measured object with strong desk lamp--the results are almost the same. This shows that the interference from the ambient light has been completely immunized.

## 5.4 RESPONSE TIME AND BANDWIDTH

For most situations encountered in the pavement measurement, the reflectivity change caused by color and slope is between 5% and 50%. The corresponding voltage variation at the input of PID control loop is about 0.5V. Table 5.1 lists the voltages at the input of PID, associated with different colored surfaces.

Table 5.1 Voltage values of the signal $\Sigma I$ with different reflectivity materials

| | Black (asphalt) | Brown (pebble) | Gray (concrete) | Yellow | White |
|---|---|---|---|---|---|
| Voltage at the input of PID (V) | 0.697 | 0.810 | 1.310 | 4.113 | 4.536 |

Figure 5.13 is the experiment results of the response time to the surface changes from the concrete color to pebble color. When the input signal at the input of PID varies, the PID auto-gain then adjusts to follow this signal change. According to the definition of the response time, the transient process spends 7 points to research the stable state (90%). The equivalent response time is (i.e. 7×5.6μs = 39.2μs), which corresponds to the bandwidth of 25.5kHz.

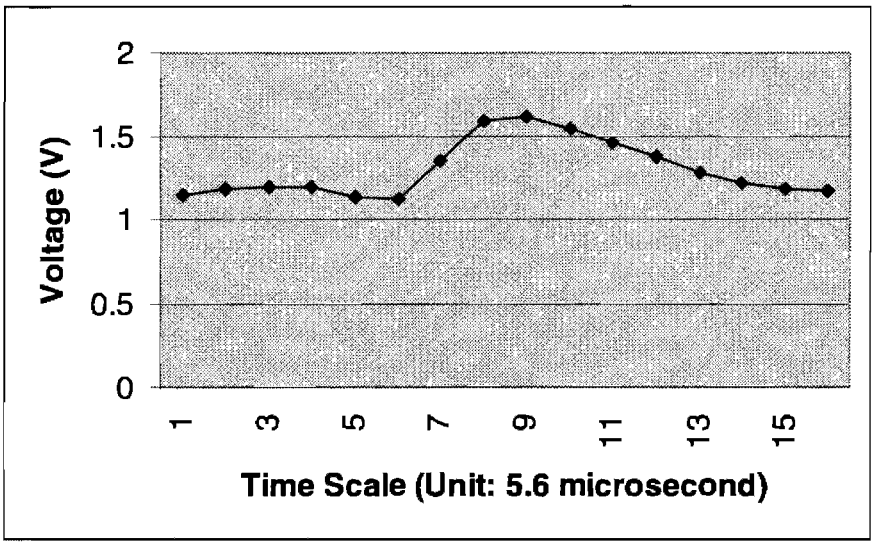


(a) Response time test 1: PID input.

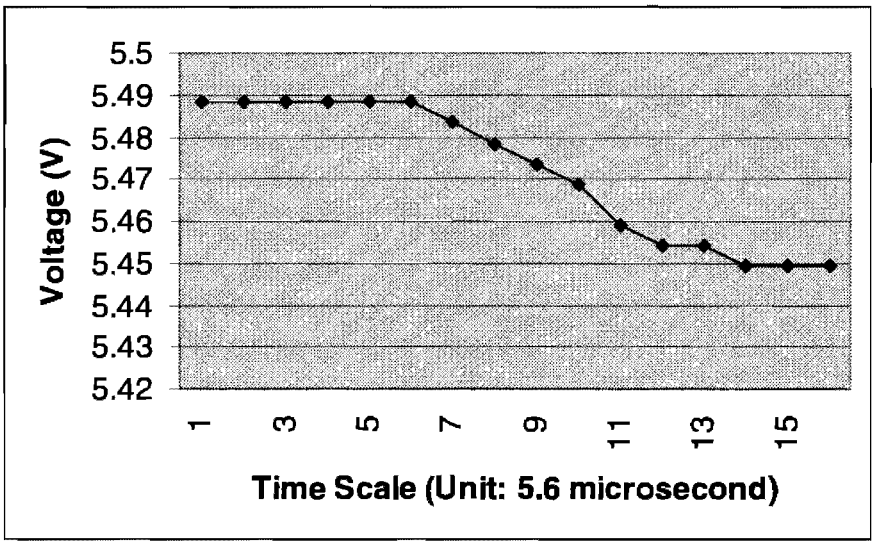


(b) Response time test 1: PID output.

Figure 5.13 Response time test 1.

Figure 5.14 is the response time as the surface changes from the pebble colour to grey colour. The transient process takes 6 points to reach the stable state (90%). The response time is (i.e. 6×5.6μs = 33.6μs), which corresponds to the bandwidth of 29.7kHz.

For the situation of slope variation (less than 45°), the voltage change is less than 0.5V at the PID input. The system can adjust the output voltage at a higher speed, as shown in Figure 5.8.

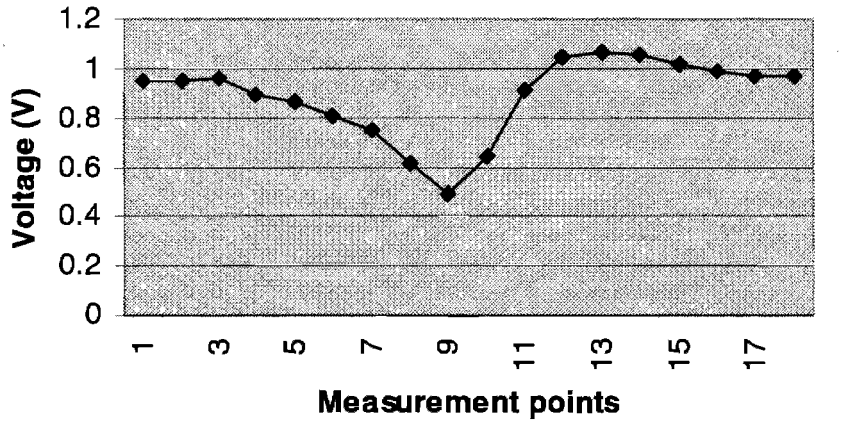


(a) Input signal of PID.

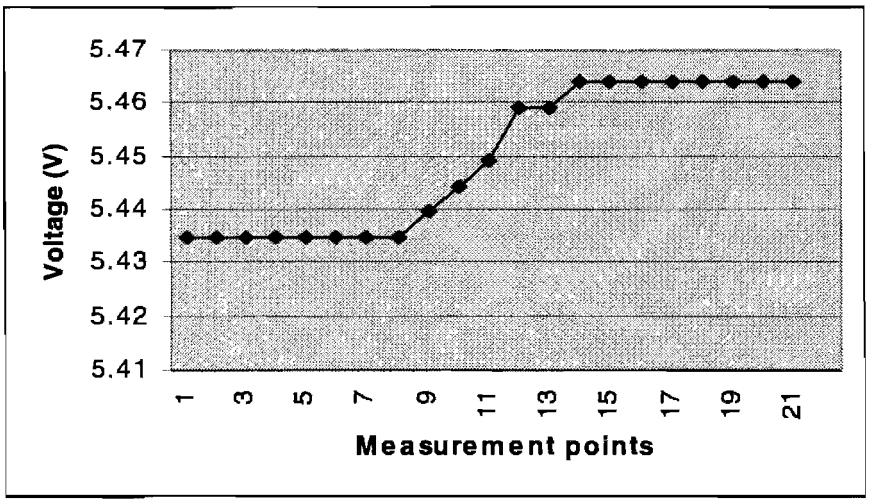


(b) Output voltage of PID control.

Figure 5.14 Response time test 2.

To test the capability limitation of the system, two extreme cases are studied. Figure 5.15 is to test the response time as the background color changes from a light color (yellow) to a dark color (dark gray). The input voltage value increases from 1.1V to 3.9V (actually, if the PID loop is open, the voltage should be 0.696V and 4.113V, respectively, which results in a 3.4V difference.) The transient time is 9 points (9×5.6μs = 50.4μs), which corresponds to the bandwidth of 19.8kHz.

Figure 5.16 shows the results when the background color suddenly changes from white color to concrete gray. The input voltage drops from 0.9V to 0.4V (in the case of PID loop open, the voltage should be 4.536V and 1.257, respectively. In general, the PID loop is closed. So this laser measurement system is not sensitive to color change.) The transient time takes 22 points (22×5.6μs = 123.2μs), which matches the bandwidth of 8.12kHz. The slow response time may be caused by the slow leaking rate of the capacitor.

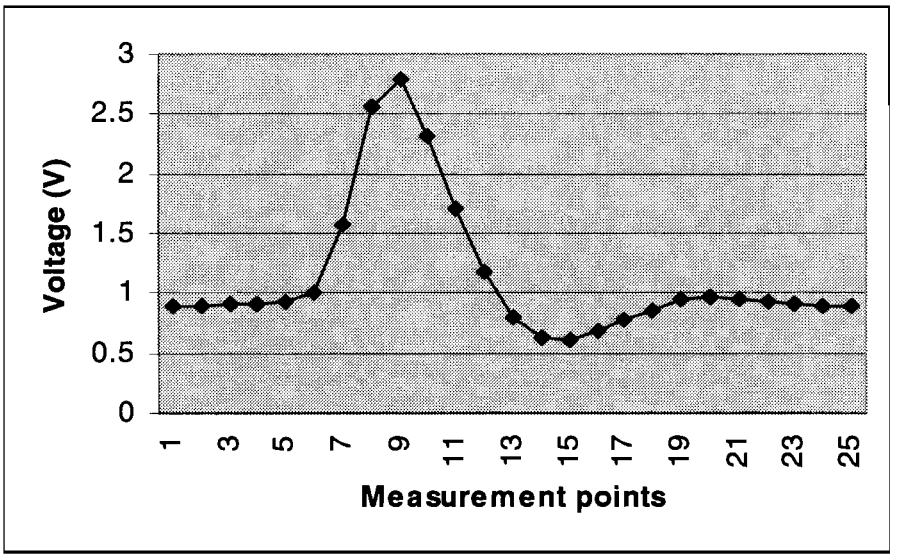


(a) Input signal of PID.

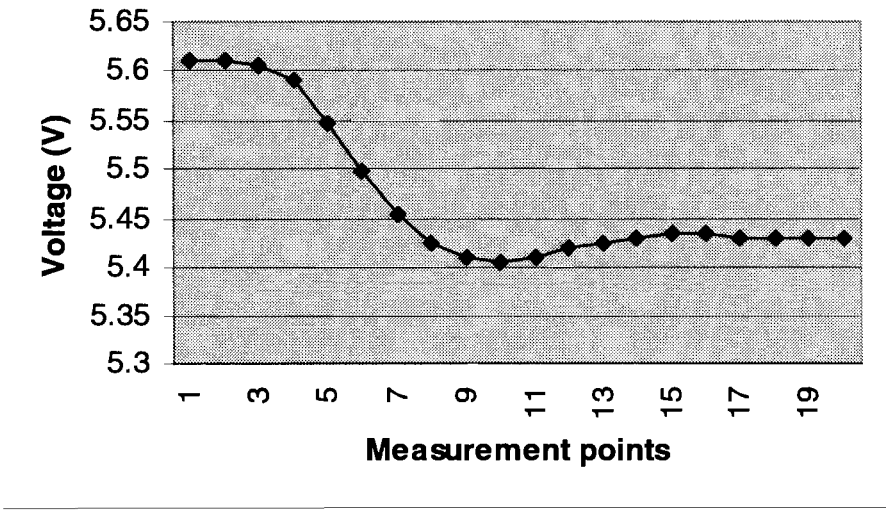


(b) Output voltage of PID.

Figure 5.15 Response time test 3.

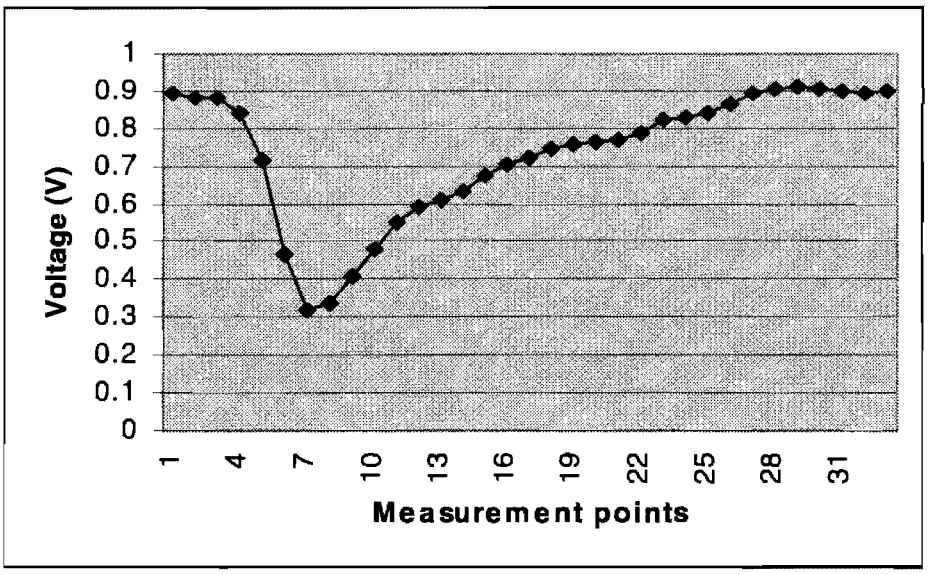


(a) Input signal of PID.

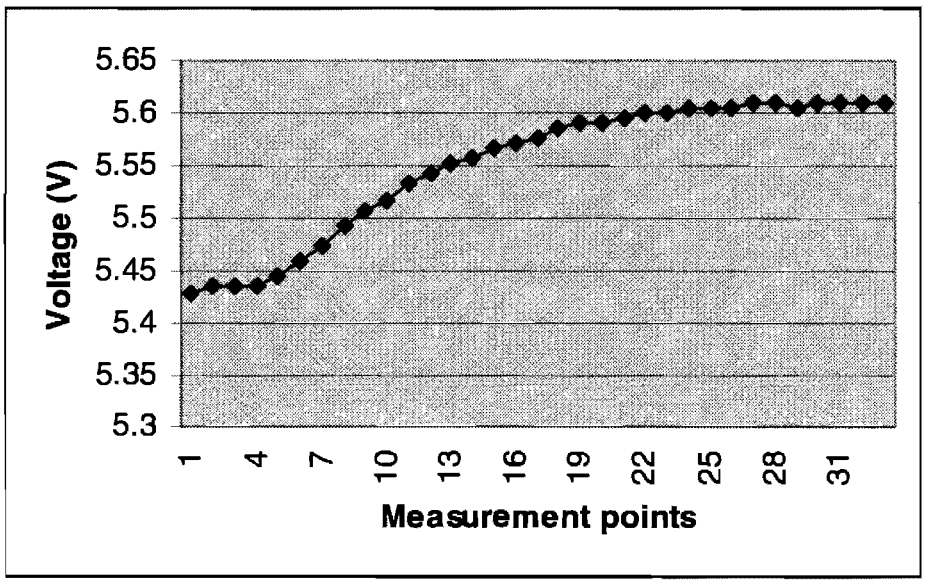


(b) Output voltage of PID.

Figure 5.16 Response time test 4

## 5.5 ANALYSIS OF MEASUREMENT ERROR

As shown in previous experiments, the errors are introduced in several aspects. In general, the measurement errors appear in the following cases:

1) Sudden slope or color changes. In this case, the system needs a short time to adjust the PID auto-gain and adapt to the changed situation. The signal cannot correctly reflect the actual profile during this period.

2) The obstacle blocks the light reflected to the PSD. Figure 5.17 illustrates this situation. The PSD cannot receive the signal and a wrong measurement result is generated at the output.

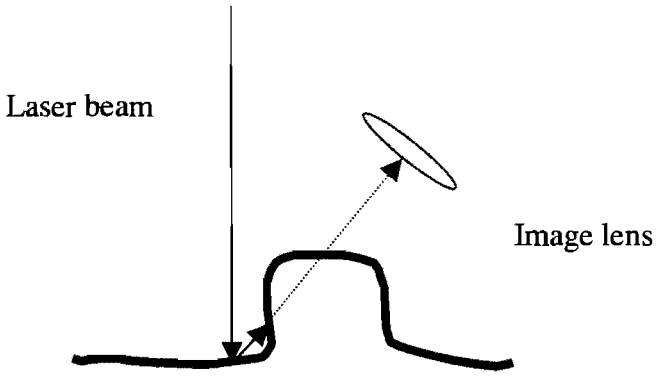


Figure 5.17 Blocked reflected light.

3) The dimension of the object to be measured is much smaller than the laser beam size. As mentioned in Chapter 3, the light intensity of the laser beam has a centroid in its circular distribution. However, if the dimension of the tiny particle is less than half of the beam spot size (the dimension of the laser beam spot should be 0.4mm), the PSD will not be able to sense the shift of the centroid. Thus, a wrong measurement would be acquired.

4) Large angled facet increases the measurement error. Figure 5.18 illustrates this phenomenon. The reflected energy is too weak for the PSD to sense the signal. Although the auto-gain of PID control can be increased to 10 times of its normal output, such situation is still beyond its capability.

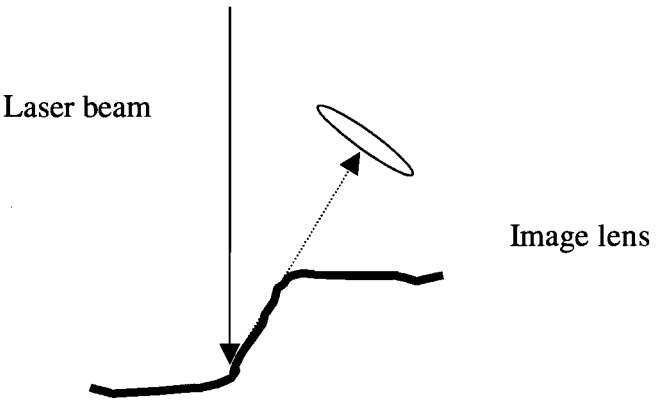


Figure 5.18 Steep slope surface.

5) The measurement on a pure black surface brings more errors. This is due to the very low reflectivity of the pure black surface, where reflectivity is usually less than 5%. Such a low reflectivity greatly reduces the light intensity reflected into the image lens and introduces bigger noise in the signal, which results in a greater measurement error.
6) Figure 5.19 and 5.20 show the pictures of the hardware system. It is seen that the laser system is compact and reliable. However, more detailed work needs to be done such as tough casing, vehicle mounting frames, and industrial grade PC for data acquisition.

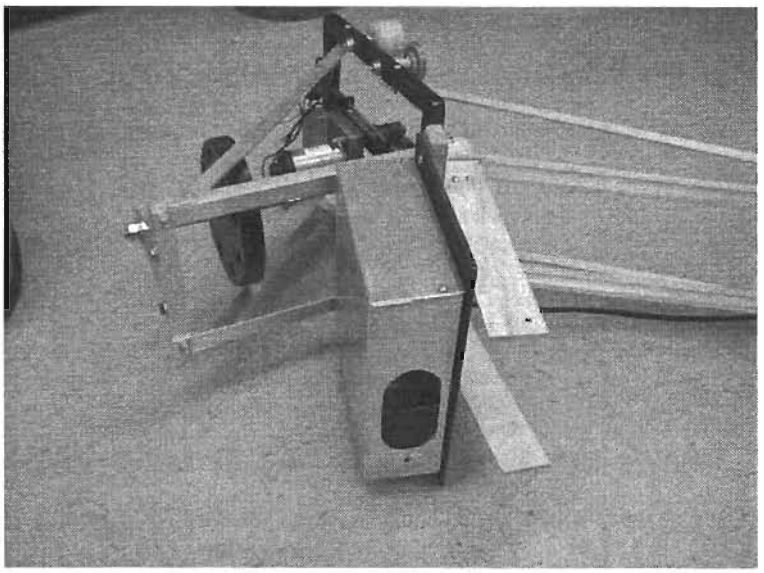

Figure 5.19 Laser sensor with mounting hardware

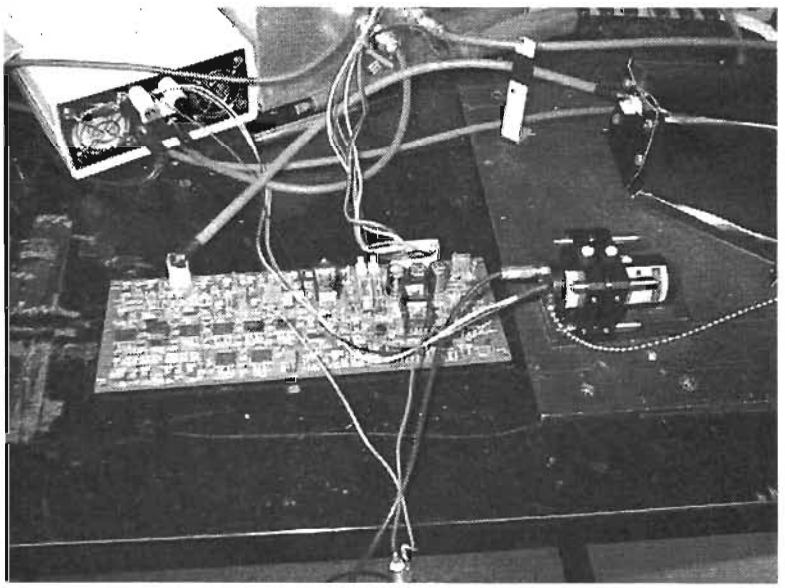

Figure 5.20 The laser sensor circuit board

# CHAPTER 6

# MICROWAVE TEXTURE MEASUREMENT SYSTEM

## 6.1 INTRODUCTION

Microwave techniques have been adopted in electronics and industries for many years, especially in remote sensing. Microwave radar and radiometers offer enhanced sensitivities to the geometrical characteristics of the earth's surface and its cover, and provide high-resolution imagery of the earth's surface.

The back-scattering radar waves are very sensitive to the geometrical features of the earth's surface as well as the geometrical structure and nature cover. The texture measurement system using a microwave sensor is to transmit a microwave signal at proper frequency, receive the scattered field by the pavement surface, and then converted the measured EM field quantities to the characteristics of the pavement surface texture.

## 6.2 BASIC MECHANISM

Any interface separating two media with different electric or magnetic properties will affect an electromagnetic wave incident on it, which is reflected according to well-known laws: the reflected field depends on the wavelength, the angle of incidence and the electrical properties (permittivity, permeability and conductivity) of two adjoining media.

What will happen if we apply the electromagnetic wave to the irregular or random variations of height measured from a certain mean plane surface, or simply rough? Usually, the difference in the behavior of a smooth and a rough surface is the fact that a smooth surface (of sufficient large dimensions) will reflect the incident wave in a single direction, while a rough surface will scatter it into various directions, though certain privileged directions we may receive more energy than others (Figure 7.1).

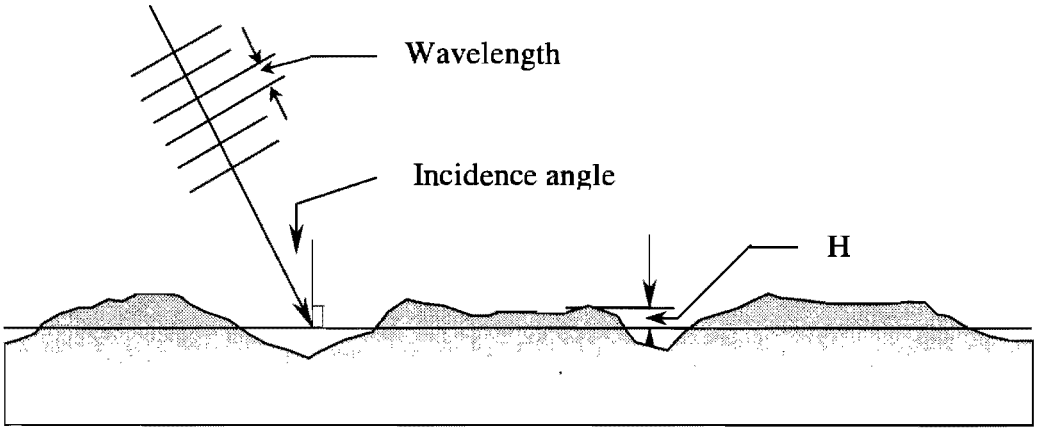


Figure 6.1. Roughness surface.

Of particular interest for the remote sensing radar is the amount of energy scattered back toward the detector. This is characterized by the surface backscatter cross section $\sigma(\theta)$[34][35]. The goal of our project is to develop a method to detect the roughness and the dielectric constant of the pavement surface.

Since the surface roughness is at the order of millimeter, so the best choice is to use high frequency electrical magnetic wave at microwave range. We have developed an algorithm to calculate the roughness and the dielectric constant if the scattering data is available. Following is the brief introduction of our project.

## 6.3 MATHEMATIC CHARACTERISTICS OF ROUGH SURFACES

Surface texture can be considered a particular rough surface. To mathematically characterize the rough surface, we need a definition of the surface roughness. Statistically, the roughness can be characterized by the standard deviation of the surface texture.

$$\sigma = \sqrt{< (z(x, y) - \overline{z(x, y)})^2 >} \qquad (6.1)$$

We can further assume that the mean of the rough surface is zero. This can be done by subtraction of the nonzero mean from the surface height to generate a zero mean rough surface. By doing this, we can greatly simplify the computation. Since in nature, most random distributed rough surfaces follow the Gaussian distribution. For one-dimensional case, the distribution function is:

$$p(z) = \frac{1}{\sigma\sqrt{2\pi}} \exp(-(z-a)^2 / 2\sigma^2) \qquad (6.2)$$

## 6.4 COMPUTATION OF THE FIELDS SCATTERED BY THE PAVEMENT SURFACE

### 6.4.1 FORWARD MODELING AND INVERSION THEORY

The computation of the rough surface parameters can be divided into two steps. The first step is to calculate the EM field scattered from the surface assuming the parameters of the rough surface is known. This step is called forward modeling. The second step is to extract the physical parameters from the measured EM waves. This step is called inversion. In this section, we discuss both forward modeling and inversion algorithms. When we calculate the scattering field from a rough surface, Kirchhoff approximation is used. The Kirchhoff integration is:

$$E2(p) = \frac{1}{4\pi} \iint_S (E \frac{\partial \phi}{\partial n} - \phi \frac{\partial E}{\partial n}) dS \qquad (6.3)$$

Where E2(p) is the electrical field at the observation point p. E is the field on the surface. $\phi$ is the Green's function of the point source. The integration goes through the whole surface (Figure 6.2).

$$\phi = \frac{\exp(ik_2 R')}{R'} \qquad (6.4)$$

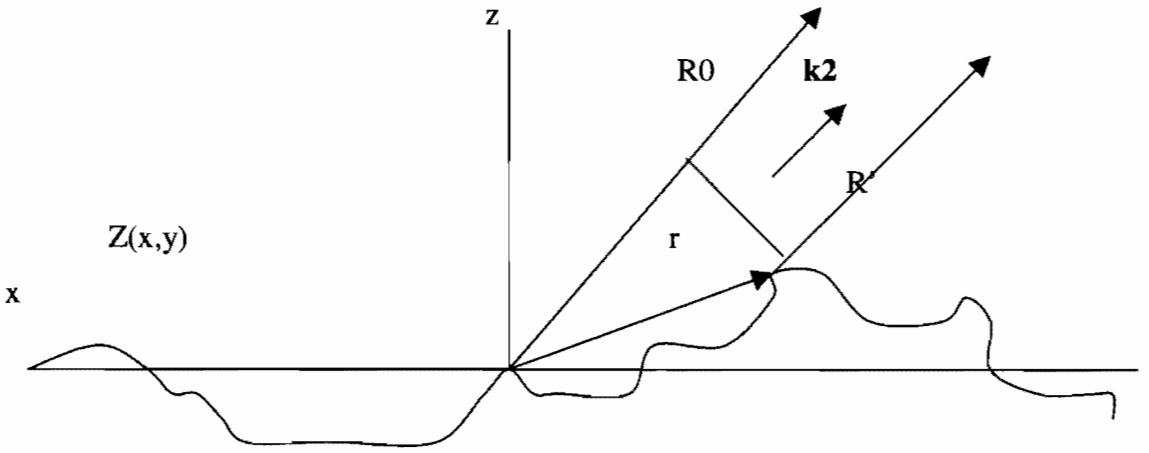


Figure 6.2. Modeling the rough surface with plan wave

We assume our incident wave is a plane wave. It is a good approximation if the source is in far-field zone. By tangential plane approximation, we can express the field on the surface by the incident wave.

$$E_S = (1+R)E_1$$
$$(\frac{\partial E}{\partial n})_S = i(1-R)E_1\vec{k}_1 \bullet \vec{n} \qquad (6.5)$$

where R is the Fresnel reflection coefficients. Depend on the polarization, R's expression is:

$$R^+ = \frac{Y^2\cos\vartheta - \sqrt{Y^2 - \sin^2\vartheta}}{Y^2\cos\vartheta + \sqrt{Y^2 - \sin^2\vartheta}}$$
$$R^- = \frac{\cos\vartheta - \sqrt{Y^2 - \sin^2\vartheta}}{\cos\vartheta + \sqrt{Y^2 - \sin^2\vartheta}} \qquad (6.6)$$

where "+" and "-" signs correspond to horizontal and vertical polarization. Y is the normalized admittance of the layer.

$$Y = \sqrt{\frac{\varepsilon_{rc}}{\mu_{rc}}} \tag{6.7}$$

After plugging in all the parameters, we have the scattered field at the observation point P as:

$$\rho = \frac{1}{4XY\cos\theta_1}\iint_S (aZ'_X + cZ'_Y - b)\exp(i\vec{v}\bullet\vec{r})dxdy \tag{6.8}$$

where **v** is the wave number difference between the incident and scattered wave.

$$\vec{v} = k[(\sin\theta_1 - \sin\theta_2\cos\theta_3)\vec{x}_0 - \sin\theta_2\sin\theta_3\vec{y}_0 - (\cos\theta_1 + \cos\theta_2)\vec{z}_0]$$
$$a = (1-R)\sin\theta 1 + (1+R)\sin\theta_2\cos\theta_3$$
$$b = (1+R)\cos\theta_2 - (1-R)\cos\theta_1$$
$$c = (1+R)\sin\theta_2\sin\theta_3$$

By inspection, it is very difficult to carry out the integral because of two derivation terms. These two terms depend on the local incident angle $\vartheta$. Meanwhile $a$ and $c$ contain the depolarization effect.

Because of the difficulty of the integration, further assumption is needed. For a random surface, the local slope is a random variable also, and its mean is zero. So we can assume that for the whole surface, the overall local incident angle effect is equal to the incident angle of the surface $\theta_1$. This is equal to replace the local incident angle $\vartheta$ in R by $\theta_1$. So a,b,c are all constant.

After this, we can easily carry out the integration.

$$\rho(\theta_1,\theta_2,\theta_3) = \frac{1+\cos\theta_2\cos\theta_1 - \sin\theta_1\sin\theta_2\cos\theta_3}{\cos_1(\cos\theta_1+\cos\theta_2)A}\iint_S \exp(i\vec{v}\bullet\vec{r})dxdy$$
$$= \frac{F(\theta_1,\theta_2,\theta_3)}{A}\iint_S \exp(i\vec{v}\bullet\vec{r})dxdy \tag{6.9}$$

In practice, it is power that we can measure easily, so we need calculate the power at the observation points. We define a new variable mean square P as:

$$P =< \rho\rho^* >$$

This mean square value is the power we measure in lab.

It is easily to be shown that:

$$P = \frac{F^2}{A^2} \int_{-X}^{X} \int_{-X}^{X} \int_{-Y}^{Y} \int_{-Y}^{Y} \exp[iv_X(x1 - x2) + iv_Y(y1 - y2)]dx1dx2dy1dy2 < \exp(iv_Z(z1 - z2)) > \tag{6.10}$$

We introduce the distance variable t so that:

$$x1 - x2 = t\cos\varphi$$
$$y1 - y2 = t\sin\varphi$$

and $< \exp(iv_Z(z1 - z2)) >= \int_{-\infty}^{\infty} \int_{-\infty}^{\infty} f(z1, z2)\exp(iv_Z(z1 - z2))dz1dz2 = \chi(vz, -vz)$ is the characteristic function associated with the distribution function f(z1,z2).

For a two dimensional Gaussian distribution, we have

$$f(z1, z2) = \frac{1}{2\pi\sigma^2\sqrt{1 - C^2}} \exp[-\frac{z1^2 - 2Cz1z2 + z2^2}{2\sigma^2(1 - C^2)} \tag{6.11}$$

where C is the autocorrelation coefficient and

$$C = \exp(-t^2 / T^2)$$

T is the autocorrelation distance. By choosing the different T and $\sigma$, we can describe all kind of the Gaussian random surface.

After some manipulation, we have our result as:

$$< \rho\rho^* >= \exp(-g)(\sin cv_X L + \frac{\sqrt{\pi}F^2T}{2L} \sum_{m=1}^{\infty} \frac{g^m}{m!\sqrt{m}} \exp(-v_x^2 T^2 / 4m) \tag{6.12}$$

where $\sqrt{g} = v_Z\sigma = 2\pi\frac{\sigma}{\lambda}(\cos\theta_1 + \cos\theta_2)$

### 6.4.2 COMPUTATION RESULTS

After we have the theory, we implemented a computer code to calculate the scattered field from the rough surface. The program includes a forward and an inversion subroutine. In forward model, we use the dielectric constant $\varepsilon$, the standard deviation $\sigma$ and the autocorrelation distance T as input to calculate the power on any observation point. Since depolarization will make the calculation difficult, we restrict the observation points within the incident plane ($\theta_3 = 0$).

In inversion model, we have 3 data measured at different receiving points with the incident source fixed. By using these 3 sets of data, program can give $\sigma, T, \varepsilon$ as the output.

#### 6.4.2.1 FORWARD MODELING RESULTS

Figure 6.3, 6.4, and 6.5 show the received scattered field power as a function of the receiving angle when transmitter incident angle is 10, 20, and 30-degree, respectively.

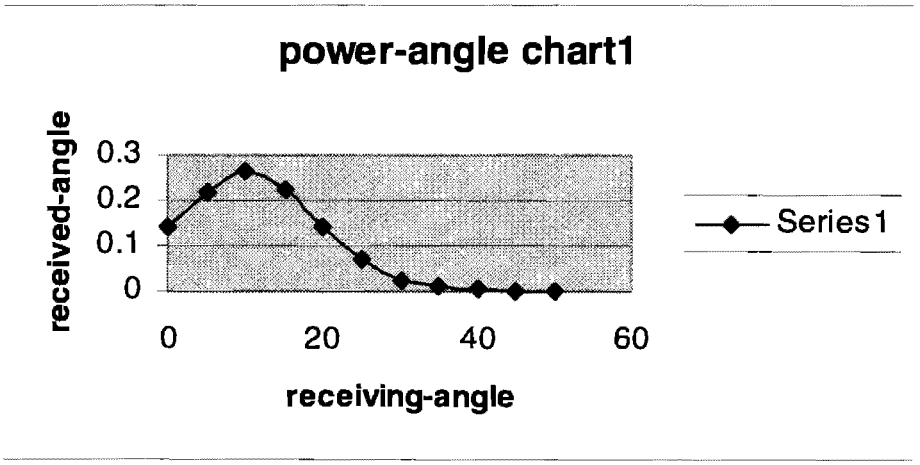


Figure 6.3 Received scattering power versus receiver angle when the incident angle is 10 degrees when the surface is smooth.

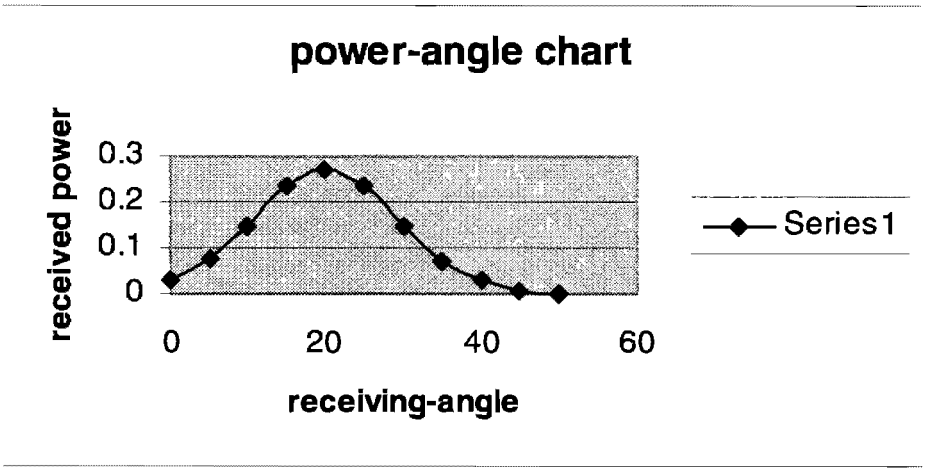


Figure 6.4 Received scattering power versus receiver angle when the incident angle is 20 degrees when the surface is smooth.

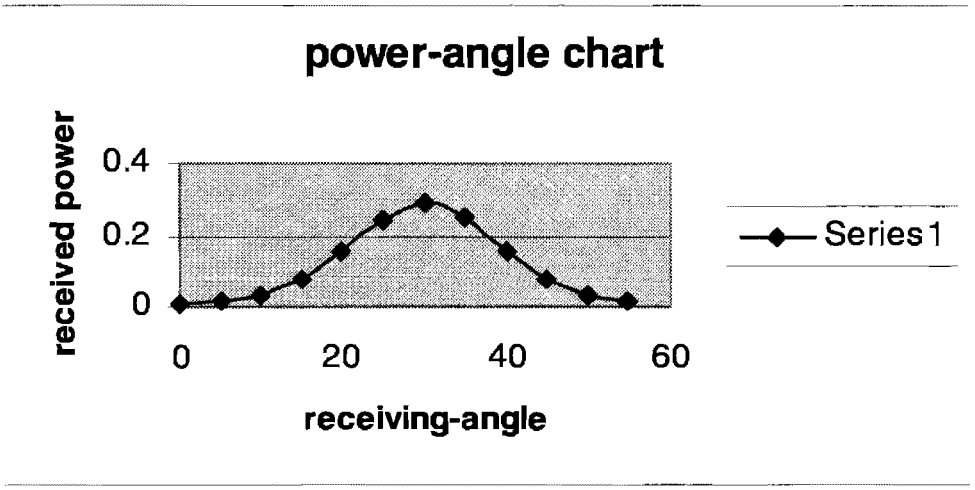


Figure 6.5 Received scattering power versus receiver angle when the incident angle is 30 degrees when the surface is smooth.

From 6.3-6.5, we can see that the maximum power occurs at the reflection angle (10,20,30 degree respectively). If surface is smooth, received power will decrease

quickly to zero. With certain degree of roughness, we can have none-zero power distribution in whole half space.

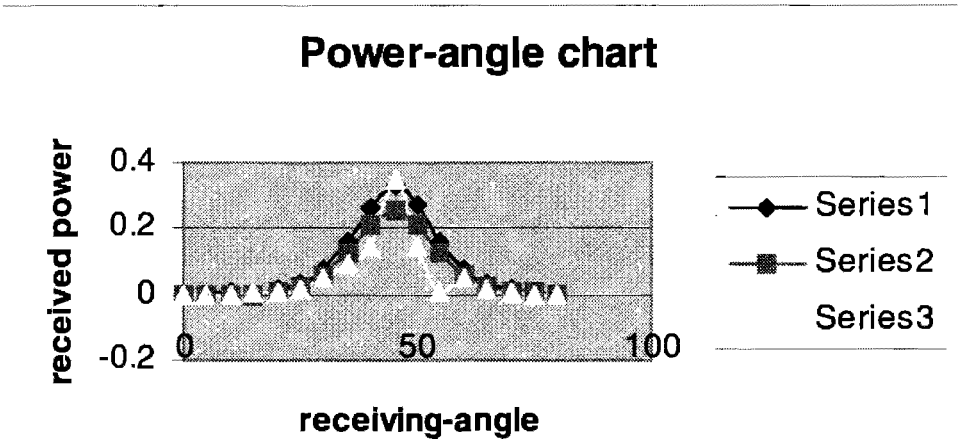


Figure 6.6 Received power changes with angle when roughness=3mm, correlation distance=5cm, dielectric constant equal to 10,8,6 respectively

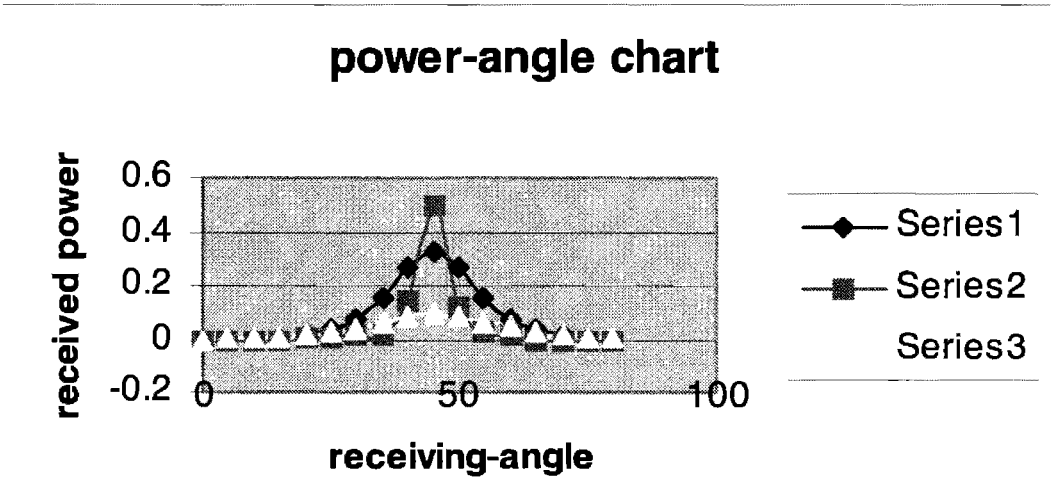


Figure 6.7 Received power changes with angle when roughness=1,3,5mm respectively, dielectric constant=10, correlation distance=5cm

From Figure 6.6 and 6.7, we can see that when we change one parameter, the spatial power distribution is changed drastically. So the power distribution is very sensitive to the surface characteristic.

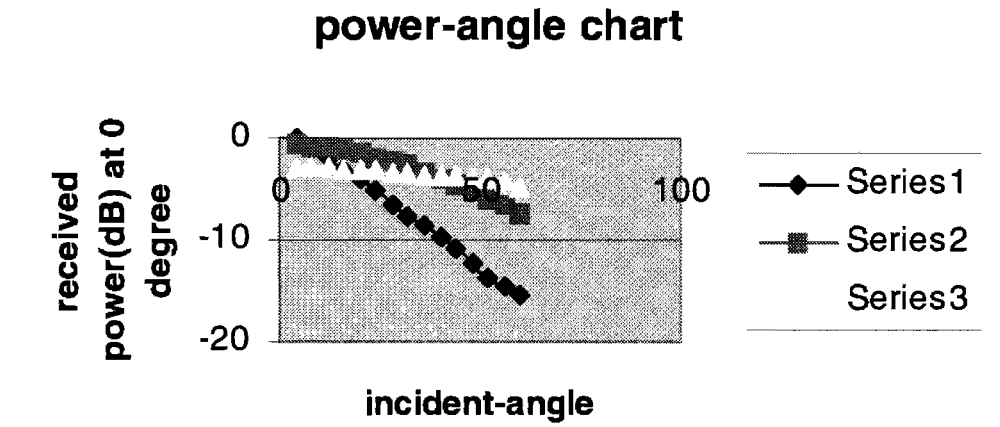


Figure 6.8 Power-incident angle relations with receiving point fixed (0 degree) while roughness =1,3,5 mm respectively, dielectric constant=10, correlation distance=5cm

From Figure 6.8, we can see when incident angle changes, different parameter results in different result at the same observation point. After analysis the above result, we found that the scattering wave spatial distribution is sensitive to the surface characteristics. So we can develop an inversion method to obtain the desired parameter from experimental data.

### 6.4.2.2. INVERSION RESULTS

Inversion subroutine takes experimental data as input to calculate the roughness, dielectric constant and correlation distance. Firstly, we randomly choose three values as our initial guess for the three parameters. Each iteration will generate a certain correction to our initial guess. Least square method has been used as our termination criterion.

Two experiments have been performed. The result is shown in Table 6.1.

Table 6.1 Inverted Pavement Roughness from Measured Data

| Roughness (mm) | Dielectric constant | Correlation distance (mm) | Actual roughness (mm) | Number of Iterations |
|---|---|---|---|---|
| 11.25 | 9.47 | 80.23 | 1.87 | 9 |
| 11.89 | 9.50 | 90.12 | 1.87 | 10 |

Although dielectric constant and correlation distance looks reasonable, the roughness value is not ideal. In this experiment, actual roughness is obtained by laser texture sensor.

## 6.5 FOCUSED MICRWAVE TEXTURE SENSOR

### 6.5.1 MICROWAVE LENS FOR SURFACE ROUGHNESS MEASUREMENT

When a beam of microwave incident on the surface of the pavement, part of the microwave energy will be scattered or reflected back [36]. The strength and the phase of the reflected wave partially depend on the roughness of the pavement surface. The roughness of the pavement surface can then be detected by properly processing the received reflections as analyzed in previous sections. A schematic of the measurement system is shown in Figure 6.9. However, the accuracy of the measured roughness may be affected seriously by the following signal passes (indicated by dashed arrows in Figure 6.9):

(1) Direct couplings between the transmitting antenna and the receiving antenna;

(2) Reflected waves from areas other than the interested spot.

Note that the reflected signal is not the desire signal because it is a strong function of the surface reflection coefficient and a weak function of the roughness (scattering).

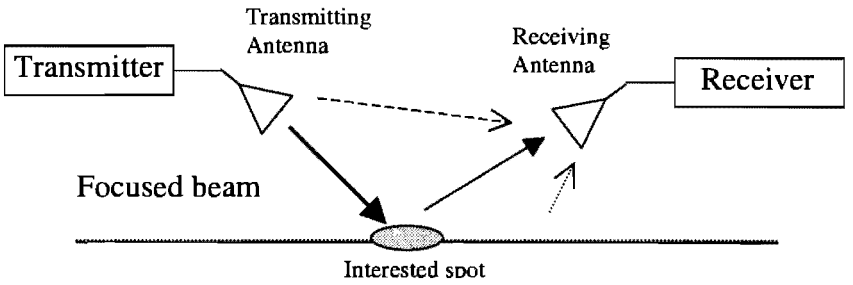


Figure 6.9 Schematic of roughness measurement system with focused antennas

To overcome the above problems, we designed and fabricated microwave lenses. With the microwave lenses, the radiated waves from the transmitting antenna can be focused to a very small spot on the pavement, and the receiving antenna can also be made to receive the signals from a very small refection spot. In this way, the direct coupling between two antennas through side lobes can be dramatically reduced. Both transmitting and receiving antennas can be focused on the interested detecting spot. The measurement system becomes more efficient with focused lenses. The following two sections will give the design and measurement results in detail.

### 6.5.2 DESIGN OF THE MICROWAVE LENS

The dielectric lens is employed in this application. The structure of the lens is shown in Figure 6.10 with its contours $S_1$ and $S_2$ represented by $(x_1, y_1)$ and $(x_2, y_2)$, respectively.

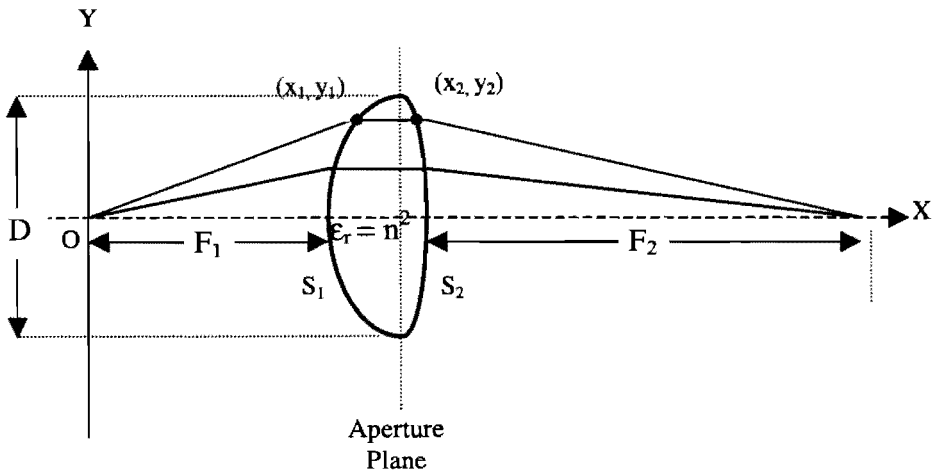


Figure 6.10 Geometry for the dielectric lens

The lens is rotationally symmetric, and therefore only the cross section of it is of interest. The principle of designing the lens is to find out the following two functions for describing the contours $S_1$ and $S_2$,

$$\begin{cases} y_1 = f(x_1) \\ y_2 = g(x_2) \end{cases} \tag{6.13}$$

such that each ray path passing through the lens has the same optical length. After mathematical derivations, a simple solution can be obtained as:

$$\begin{cases} x_1(y) = \dfrac{nF_1 + \sqrt{F_1^2 + \dfrac{(n+1)\,y^2}{n-1}}}{n+1} \\ x_2(y) = x_1(\dfrac{D}{2}) + \dfrac{\sqrt{F_2^2 + \dfrac{(n+1)D^2}{4(n-1)}} - \sqrt{F_2^2 + \dfrac{(n+1)\,y^2}{n-1}}}{n+1} \end{cases} \tag{6.14}$$

The shape of $S_1$ is designed to pick up the microwave with a phase center at the apex of the horn antenna and to obtain a uniform phase distribution on the antenna aperture. The shape of $S_2$ is designed to focus the uniformly distributed microwave at the aperture to a given interested spot.

According to the size of the horn antennas, the parameters of the lens are chosen as the Table 6.2. Notice that the lens design is based on optical ray approximation and is not frequency dependent. In other words, the lenses designed for 10 GHz system can also be used in 100 GHz system as long as the material used for lenses does not present high loss at 100 GHz. The material used is fiberglass epoxy.

Table 6.2 Parameters of Microwave Lens

| $F_1$ (inch) | $F_2$ (inch) | D (inch) | $\varepsilon_r$ ($n^2$) | Test Frequency (GHz) |
|---|---|---|---|---|
| 4.72 | 9.84 | 2.87 | 4.10 | 10, 35, 100 |

The microwave lenses were fabricated according the above parameters and shapes given by Equation (6.14). Figure 6.11 is a photograph of the microwave lens.

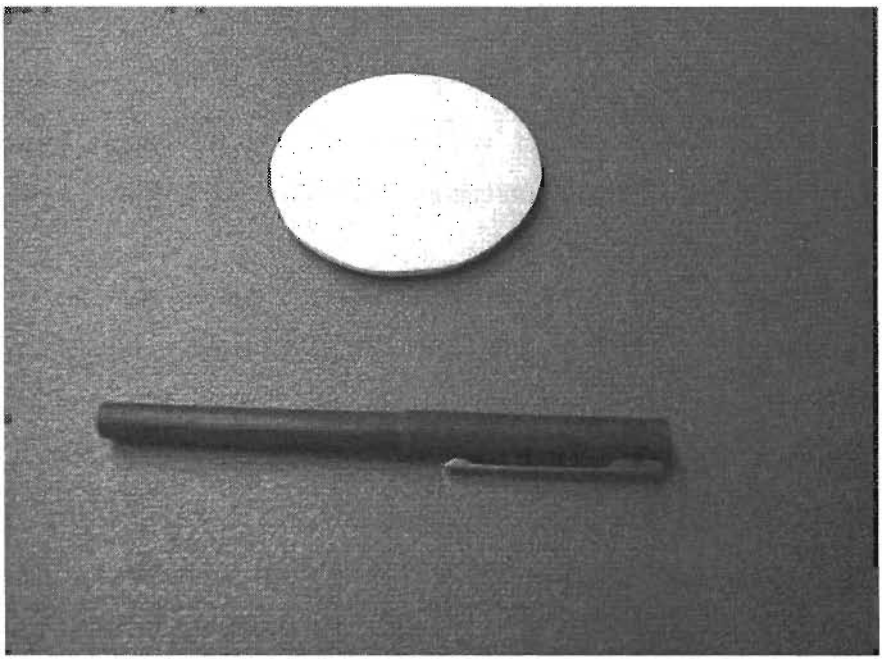

Figure 6.11 Microwave lens manufactured using glass epoxy

### 6.5.3 LAB TEST RESULTS

Before applying the system to the practical measurements, we need to know how large an area the system can detect. Hence we mounted the system one-meter high above the pavement surface (in this case nothing reflects waves from the focusing zone to the receiving antenna), we move a very small piece of metal along x-axis and y-axis, respectively, in the focusing plane. The center of the focusing zone is chosen as origin of the coordinates. The measured results are given in Figure 6.12. The results show that only an area of about 4×4 square inches can be "seen" by the system at each measurement.

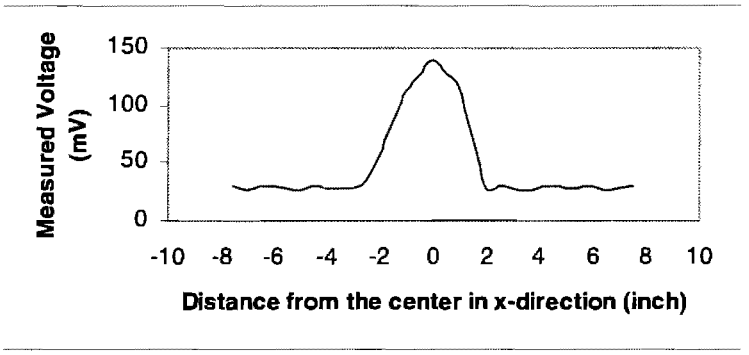


(a)

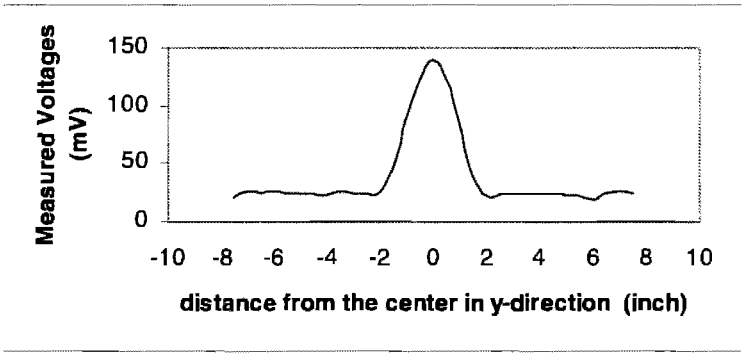


(b)

Figure 6.12 Sensitivity zone (a) in x-direction; (b) in the y-direction

Four concrete samples with different surface roughness are tested. The results are given in Figure 6.13. The rougher the surface is, the larger the scattered signal from the surface. The textures of the samples are characterized by using the laser profiler. The roughness distribution function is Gaussian and the correlation length is in the range of 80- 90-mm, and the roughness is 1.2 – 2.5 mm. The experiment show that the microwave sensor is very sensitive to surface texture. The received power is linearly related to the surface roughness.

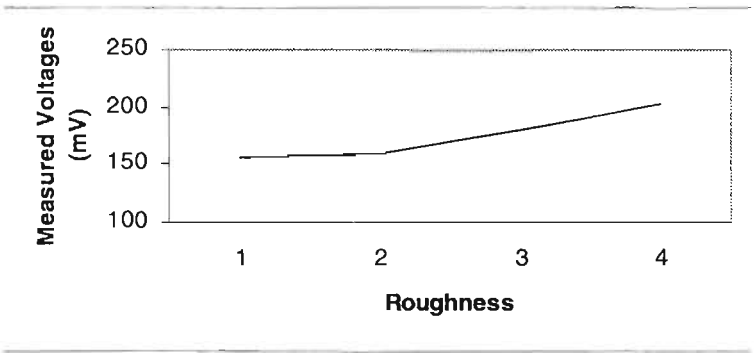


Figure 6.13. Relations between the scattered field and the roughness of the concrete surface

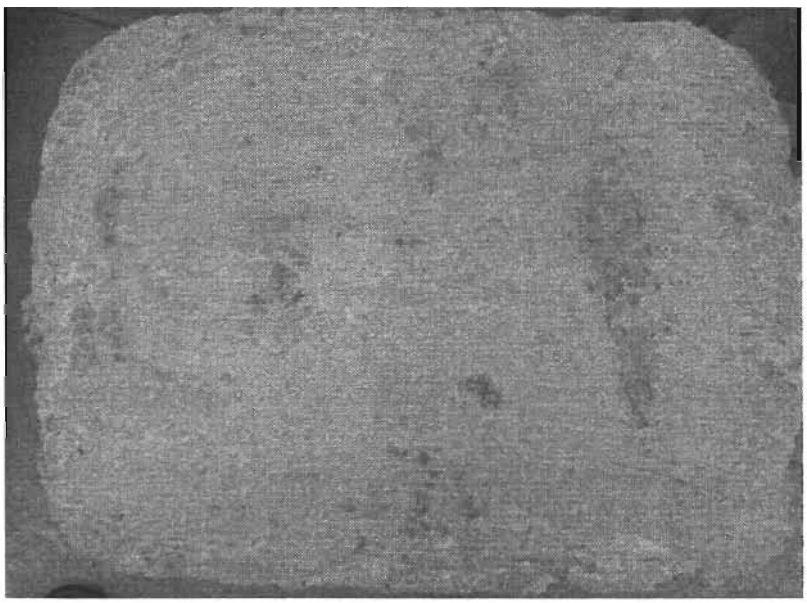

Figure 6.14 Example of the sample surface used in the tests

## 6.6 SUMMARY

The microwave sensor for pavement texture is very potential in detecting macro texture. Experiment results show that the system can be easily implemented for TxDOT network level projects. The set up can be very simple and straightforward using dielectric lenses. However, more work must be done to combine the sensor with a distance measurement tool. In this study, a numerical method has been developed to get random rough surface parameter. The

computation result has certain degree of error. When we perform the Kirchhoff integration, we only consider the average effect of the local incident angle, so the integration can be carried out easily. This certainly will introduce error in our result. To improve the result, we should include the local incident angle effect, the price we will pay is that the computation time will increase since we can not avoid the numerical integration.

**REFERENCES:**


[1] Nicholas J. Garber, Lester A. Hoel, Traffic and Highway Engineering, 2nd Ed., PWS Publishing Co., New York, 1997.

[2] Evans, D.L., T. G. Farr, and J.J. van Zyl, "Estimates of surface roughness derived from synthetic aperture radar (SAR) data, IEEE Trans. Geosci. Remote Sensing, GE-30, no.2, 382-389, 1992.

[3] Donald R. Wehner, High Resolution Radar, 2nd Ed., Artech House, Boston, 1995.

[4] Micropower Impulse Radar (MIR), Internet documents at Lawrence-Livermore National Lab. Site (http://lasers.llnl.gov/lasers/idp/mir/files/MIR_info.html), 1996.

[5] I-B. Kong and S-W. Kim, "Portable inspection of precision surfaces by phase-shifting interferometer with automatic suppression of phase-shift errors," Optical Engineering 34, 1400-1404, (1995).

[6] J. van Wingerden, H. J. Frankena, and B. A. van der Zwan, "Optical profiler for low-reflectance ultra-smooth surfaces," Optical Engineering 31, 2450-2457, (1992).

[7] CCD Sensors and Cameras, Product Catalog, Dalsa Inc., Waterloo, Ontario, Canada, 1997.

[8] Robert J. Schalkoff, Digital Image Processing and Computer Vision, John Wiley, New York, 1989.

[9] Michael A. Paesler and Patrick J. Moyer, Near-field Optics: Theory, Instrumentation, and Applications (Wiley-Interscience, New York, 1996).

[10] Gerald V. Blessing, John A Slotwinski, Donald G. Eitzen, and Harry M. Ryan, "Ultrasonic measurements of surface roughness," Applied Optics 32, 3433-3437 (1993).

[11] Measuring & benefits, Selcom, No.2 1997

[12] Bazin G. – Journet B, "A new laser range-finder based on FMCW-like method," IEEE Instrumentation and Measurement Technology Conference, June 4-6, 1996, 90-93

[13] Steel, W. H., "Interferometry", 2nd ed., Cambridge University Press, New York, 1986.

[14] Robert J. Dwulet, "Laser Triangulation Expands Measurement Options," Design News, Mar 27, 1995, 114

[15] Fair Lawn, "Laser Sensor Broadens sensing range," Design News, May 22, 1989, 42

[16] David R. Wiese, "Laser triangulation sensors: A good choice for high speed inspection," I&CS September, 1989, 27-29

[17] Robert W.McCullough and J.L.Doyle, "Laser-Optical Triangulation Systems Provide New Capabilities for Remote Inspection of Interior Surfaces," Materials Evaluation, Dec 1995, 1338-1345

[18] V.V.Yakolev, "High-precision laser range finders and laser systems for industrial use. –Opt. Engineering, Aug. 1994, vol 33, n°8,2754-2758

[19] R.L.Dalglish, C. McGarrity and J. Restrepo, "Hardware architecture for real-time laser range sensing by triangulation," Rev. Sci. Instrum. Vol. 65 No. 2, Feb. 1994, 485-491

[20] Selcom Inc. Opotcator Laser Sensor Manual, 1996

[21] Hamamatsu technical data about large-area PSD series, Hamamatsu Photonics K.K. 1993

[22] Instruction Manual of Signal Processing Circuits for 1-dimensional PSD, Hamamatsu Photonics K.K.

[23] Mario Tuerschmann, Peter P. Mager and Rainer Endter, "Improved Accuracy in Laser Triangulation by Variance-stabilizing transformations", Opt Engineering, July 1992, Vol. 31 No. 7, 1538-1545

[24] Manuel F. M. Costa, "Surface Inspection by an Optical Triangulation Method," Opt. Eng. September 1996, 39(9) 2743-2747

[25] T. R. Thomas, "Rough Surfaces", Longman Group Limited, London and New York, 1982

[26] Oleg V. Angelsky, "Interference Measurement of Rough Surfaces", Simulation and Experiment in Laser Metrology, Akademie Verlag, Berlin, 1996, p106-108

[27] David Beach, "Applications of Lasers and Laser System", PTR Prentice Hall, Englewood Cliffs, New Jersy, 1993

[28] Jeff Hecht, "Understanding Lasers", IEEE Press Understanding Science & Technology Series, New York, 1993

[29] Pasi Palojarvi, "Integrated Time of Flight Laser Radar", IEEE instrumentation and Measurement Technology Conference, Brussels, Belgium, June4-6, 1996

[30] Andrzelj, W. Domanski and Tomasz R. Wolinski, "Surface Roughness Measurement with Optical Fibers", IEEE, 1992

[31] Michael W. Sayers, "The Little Book of Profiling", University of Michigan, Oct. 1996

[32] Mclean, J. and Foley, G., "Road Surface Characteristics and Condition: Effects on Road Users", ARRB Transport Research Ltd., Research Report No. 314.

[33] James T. Luxon & David E. Parker, "Industrial Lasers and Their Applications", Prentice-Hall, Inc. Englewood Cliffs, New Jersey, 1984

[34] J.J. van Zyl, C.F. Burnette, and T.G. Farr, "Inference of surface power spectra from inversion of mulifrequency polarimetric radar data, Geophys. Res. Lett., 18(9), 1787-1790,1991.

[35] Wu, Z.X., and Liu, C., 1996. An image reconstruction method using GPR data, 6th International Conference on Ground Penetrating Radar, Sendai, Japan, Sept. 30.

[36] Charles V. Jakowatz, Jr., Daniel E. Wahl, Paul A. Thompson, Spotlight-Mode Synthetic Aperture Radar: A Signal Processing Approach. Kluwer Academic Publishers, Boston, 1996.